

A comparative analysis between field-oriented control and uncontrolled current operation of a brushless DC motor

by

Nahid Uzzaman

B.S., Bangladesh University of Professionals, 2016

A THESIS

submitted in partial fulfillment of the requirements for the degree

MASTER OF SCIENCE

Department of Mechanical and Nuclear Engineering
College of Engineering

KANSAS STATE UNIVERSITY
Manhattan, Kansas

2019

Approved by:

Major Professor
Dr. Dale Schinstock

Copyright

© Nahid Uzzaman 2019.

Abstract

Field-oriented control (FOC), also known as vector control is a very popular and effective way of driving a Brushless DC (BLDC) motor. However, the BLDC motor can also be run without any current controlling. In this thesis, this method is addressed as uncontrolled current operation, which is simply driving a BLDC motor in the absence of vector control. The characteristics and conditions for effective operation of the uncontrolled current are studied. The thesis discusses and models both vector control and uncontrolled current operation and describes a Simulink simulation building procedure for these two methods. An overall comparison is carried out between these two methods for various aspects, such as commutation accuracy, maximum torque production, handling of external delays, etc. In the analysis, it is seen that the vector control shows a better operating range, but the uncontrolled current shows better stability. The simulation shows that vector control cannot handle external hindrance (such as the computing delay of the controller) very well. On the other hand, the uncontrolled current can handle external delay better. This makes the uncontrolled current method suitable to be used in a microcontroller, as microcontrollers can be slow. Whereas, the vector control will require a very fast computer. As a potential application, the system with the uncontrolled current method is then simulated as laboratory equipment for an introductory control theory course. The model and simulation generated data shows a good match, which indicates uncontrolled current method can be used to build a low-cost introductory control theory laboratory equipment.

Table of Contents

List of Figures	vi
List of Tables	x
Chapter 1 - Introduction	1
Chapter 2 - Field Oriented Control Operation and Uncontrolled Current Operation	4
2.1 Field Oriented Control.....	6
2.1.1 Clarke Transformation	7
2.1.2 Park Transformation	10
2.2 Uncontrolled Current Operation	11
Chapter 3 - Building Simulation	13
3.1 State Space Formulation of the Electrical Dynamics of the Motor	13
3.2 Torque Production from Sinusoidal Currents	17
3.3 Motor Mechanical Plant	19
3.4 Vector Control.....	20
3.5 Voltage Divider	21
3.6 Back EMF	22
3.7 Simulation Models	23
Chapter 4 - Modeling and Frequency Response Analysis	28
4.1 Speed Control Model with Vector Control.....	29
4.2 Speed Control Model with Uncontrolled Current	30
4.3 Position Control Model with Vector Control.....	31
4.4 Position Control Model with Uncontrolled Current.....	33
4.5 Frequency Response of the Systems	34

Chapter 5 - Commutation	43
5.1 Actual Torque and Maximum Torque	43
5.2 Computing Delay	52
Chapter 6 - Application of Uncontrolled Current Operation.....	64
6.1 Saturation	64
6.2 Speed Control Experiment with Uncontrolled Current	67
6.2.1 Speed Control with Proportional Controller	67
6.2.2 Speed Control with Proportional-Integral Controller	70
6.3 Position Control Experiment with Uncontrolled Current	72
6.3.1 Position Control with Proportional Controller	72
6.3.2 Position Control with Proportional-Derivative Controller.....	74
Chapter 7 - Conclusion.....	76
References	78
Appendix A - Code	80
Initialization.m	80
Torque Generation	80
Back EMF	80
Voltage Divider.....	80
Clarke Transform	81
Park Transform	81
Inverse Clarke Transform.....	81
Inverse Park Transform	81
Bode Plot Generator for Section 4.5	81

List of Figures

Figure 1.1: Schematic diagram of a BLDC Motor.	1
Figure 3.1: Schematic diagram of a BLDC Motor.	14
Figure 3.2: Torque production in sinusoidal BLDC motor.	18
Figure 3.3: Speed model of the motor.	19
Figure 3.4: Simulation Model for Speed Control System with Vector Control Operation.	24
Figure 3.5: Simulation Model for Speed Control System with Uncontrolled Current Operation.	24
Figure 3.6: Simulation Model for Position Control System with Vector Control Operation.	25
Figure 3.7: Simulation Model for Position Control System with Uncontrolled Current Operation.	25
Figure 3.8: Angular Speed of the Motor with Vector Control.	26
Figure 3.9: Angular Speed of the Motor with Uncontrolled Current.	27
Figure 4.1: Speed control of a BLDC motor with vector control.	29
Figure 4.2: Speed control of a BLDC motor with uncontrolled current.	31
Figure 4.3: Position control of a BLDC motor with vector control.	32
Figure 4.4: Position control of a BLDC motor with uncontrolled current.	33
Figure 4.5: Open Loop Bode Plot of Speed Control System with Vector Control.	35
Figure 4.6: Closed Loop Bode Plot of Speed Control System with Vector Control.	35
Figure 4.7: Open Loop Bode Plot of Speed Control System with Vector Control with $K_p = 100$ and $K_i = 1000$	37
Figure 4.8: Closed Loop Bode Plot of Speed Control System with Vector Control with $K_p = 100$ and $K_i = 1000$	37

Figure 4.9: Open Loop Bode Plot of Speed Control System with Vector Control with $K_p = 1$ and $K_i = 10$	38
Figure 4.10: Closed Loop Bode Plot of Speed Control System with Vector Control with $K_p = 1$ and $K_i = 10$	38
Figure 4.11: Open Loop Bode Plot of Speed Control System with Uncontrolled Current.	39
Figure 4.12: Closed Loop Bode Plot of Speed Control System with Uncontrolled Current.	39
Figure 4.13: Open Loop Bode Plot of Position Control System with Vector Control.	40
Figure 4.14: Open Loop Bode Plot of Position Control System with Uncontrolled Current.	40
Figure 4.15: Closed Loop Bode Plot of Position Control System with Vector Control.	41
Figure 4.16: Closed Loop Bode Plot of Position Control System with Uncontrolled Current.	41
Figure 5.1: Torque Ratio Vs. Angular Speed for System with Uncontrolled Current.	47
Figure 5.2: Torque Ratio Vs. Angular Speed for System with Vector Control.	47
Figure 5.3: Calculating Phase Shifts of Motor Current.	49
Figure 5.4: Simulated Phase Shift of Current for System with Uncontrolled Current.	50
Figure 5.5: Simulated Phase Shift of Current for System with Vector Control.	51
Figure 5.6: Simulation Model with Delay for System with Uncontrolled Current.	52
Figure 5.7: Simulation Model with Delay for System with Vector Control.	53
Figure 5.8: Simulated Angular Speed of the Motor with No Delay for Uncontrolled Current System.	53
Figure 5.9: Simulated Angular Speed of the Motor with No Delay for Vector Control System.	54
Figure 5.10: Simulated Angular Speed of the Motor with 0.001 Sec Delay for Uncontrolled Current System.	54

Figure 5.11: Simulated Angular Speed of the Motor with 0.001 Sec Delay for Vector Control System.....	55
Figure 5.12: Simulated Angular Speed of the Motor with 0.0001 Sec Delay for Uncontrolled Current System.	56
Figure 5.13: Simulated Angular Speed of the Motor with 0.0001 Sec Delay for Vector Control System.....	56
Figure 5.14: Torque Ratio for Uncontrolled Current with Delay in the Simulation.....	58
Figure 5.15: Torque Ratio for Vector Control with Delay in the Simulation.	58
Figure 5.16: Simulated Phase Shift of Current with 0.0001 sec Delay for Uncontrolled Current.	60
Figure 5.17: Simulated Phase Shift of Current with 0.0001 sec Delay for Vector Control.	60
Figure 5.18: Simulated Phase Shift of Back EMF with 0.0001 sec Delay for Uncontrolled Current.	62
Figure 5.19: Simulated Phase Shift of Back EMF with 0.0001 sec Delay for Vector Control.	62
Figure 6.1: Simulation Block of Speed Control System with Voltage Saturation for Uncontrolled Current Operation.	65
Figure 6.2: Simulation Block of Position Control System with Voltage Saturation for Uncontrolled Current Operation.	66
Figure 6.3: Speed Control Responses for Command = 200 and $K_p = 0.01, 0.05$	68
Figure 6.4: Speed Control Responses for Command = 100 and $K_p = 0.005, 0.01, 0.1$	68
Figure 6.5: Speed Control Responses for Command = 50 and $K_p = 0.05, 0.1, 0.2$	69
Figure 6.6: Speed Control Responses for Command = 50 with various PI Controllers.	70
Figure 6.7: Speed Control Responses for Command = 100 with various PI Controllers.	71

Figure 6.8: Position Control Responses for Various Commands and Proportional Gains.	73
Figure 6.9: Position Control Responses for Various Commands and P-D Gains.	74

List of Tables

Table 5.1: Torque Data from Simulation of System with Uncontrolled Current.	45
Table 5.2: Torque Data from Simulation of System with Vector Control.	46
Table 5.3: Phase Shift of the Current for System with Uncontrolled Current.	49
Table 5.4: Phase Shift of the Current for System with Vector Control.	50
Table 5.5: Torque Data for Uncontrolled Current with Delay in the Simulation.	57
Table 5.6: Torque Data for Vector Control with Delay in the Simulation.	57
Table 5.7: Phase Shift of Current with 0.0001 sec Delay for Uncontrolled Current.	59
Table 5.8: Phase Shift of Current with 0.0001 sec Delay for Vector Control.	59
Table 5.9: Phase Shift of Back EMF with 0.0001 sec Delay for Uncontrolled Current.	61
Table 5.10: Phase Shift of Back EMF with 0.0001 sec Delay for Vector Control.	61
Table 6.1: Proportional Gain and Speed Command for Speed Control Experiment.	67
Table 6.2: P-I Gains and Speed Command for Speed Control Experiment	70
Table 6.3: Position Control Experiment Command and Proportional Gain.	72
Table 6.4: Position Control Experiment Command and P-D Gains.	74

Chapter 1 - Introduction

A brushless DC (BLDC) motor is a synchronous motor which is powered by switching dc power. The commutation in a Brushless DC (BLDC) motor is controlled electronically. BLDC motors can be used for a lot of purposes. An example of the use of BLDC motor can be the application in the laboratory equipment for introductory control theory course. Brush dc motors have significant non-linear friction which is hard to model [7]. Therefore, BLDC motor is a better choice for introductory level control theory course, as it doesn't possess the friction for mechanical commutation.

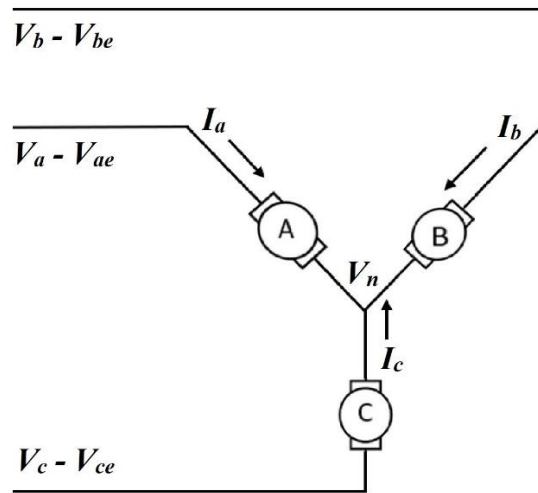


Figure 1.1: Schematic diagram of a BLDC Motor.

Laboratory work can be beneficial for the students in the introductory control theory course [1, 2, 3, 10]. However, with increasing class size, it is necessary that the number of laboratory equipment stations is also increased. But increasing the laboratory facilities comes with economic challenges. A low-cost hardware, therefore, can be beneficial to overcome such economic challenges [4, 8, 9].

One way of reducing the production cost of control system laboratory hardware is to change the operation method of the BLDC motor. For example, field-oriented control (FOC) also known as vector control is a method of driving the BLDC motor [6]. Although the vector control is a very effective [5] way of driving BLDC motor it comes with certain costs. For example, vector control needs to measure the phase currents of the motor, which adds the cost of a current sensor. If we can replace the vector control method with a different method that doesn't need to measure the motor phase currents, then we can reduce the cost of the current sensor. Such a method can be the uncontrolled current operation. As the name suggests, this method doesn't require current controlling and therefore doesn't need a current sensor.

Another way of cost reduction for the laboratory hardware can be using cheap equipment, such as cheap sensors and controllers [8]. Microcontrollers have become popular as low-cost controllers for laboratory hardware equipment [2]. However, microcontrollers have a slow clock speed. The slow speed of the microcontroller can become a problem if the system it is trying to control is faster. Thus, the system operated by a microcontroller needs to be studied.

This thesis will discuss the vector control operation and compare various aspects of this method with that of the uncontrolled current operation. Simulation models for both systems will be developed to study the systems and advantages and disadvantages of both the methods will be addressed. The aim is to replace vector control with uncontrolled current operation and describe the conditions under which this is valid. The thesis will discuss for which application and at what condition the uncontrolled current would be suitable to use. For potentially being used in the laboratory equipment of the introductory control theory

course, the performance of this method will be observed. Experiments on the system with uncontrolled current will be performed to observe the similarity between the model and simulation generated data.

Chapter 2 - Field Oriented Control Operation and Uncontrolled Current Operation

Chapter 2 will discuss the field-oriented control operation with controlling current and uncontrolled current operation. To operate a permanent magnet Brushless DC Motor (BLDC) the direction and the magnitude of the current flowing to the coils needs to be changed continuously. The rotor contains permanent magnets with opposing poles. So, the phase currents should flow in such a way that a magnetic field is produced which will attract or repel the permanent magnet and eventually make the rotor spin. Whenever a pole of the permanent magnet is near one of the stator coils, the coil should be supplied with a voltage in the direction that will produce an opposite pole which will attract the nearby magnet pole. On the other hand, if the permanent magnet pole is perfectly aligned with the stator coil, then a voltage should be supplied in the coil so that it creates the same pole as the permanent magnet and repel it. In both cases, the rotor of the motor will be moving. The direction of the rotor movement can be controlled by controlling the sequence of the voltage supplied in the stator coils.

Now, we want to maximize our energy usage. Meaning, the energy in the magnetic field, that's being generated from the electrical energy, should completely be used to turn the rotor. So, we want the torque being generated by the repulsion or attraction of the opposing or attracting poles to be maximum. The torque generated will be maximum if the permanent magnet pole and stator coil produced pole are 90° apart from each other and are opposite poles. This means the voltage should be supplied in the stator windings when the permanent magnet pole is 90° apart and the direction of the voltage should be such that it causes a current flow in a direction that will produce an opposing pole in the stator coil. This will

create an attraction force between the opposing poles and torque generated from that attraction will be maximum. The torque generated is given by the following equation [6],

$$T(\theta_r) = -k_t \sin(\theta_r).i(t) \quad (2.1)$$

Here, T is the torque generated, k_t is Per-phase torque constant, i is the current in the stator windings and θ_r is the Rotor angle. From equation (2.1) we can see that, in order for the torque generated to be maximum the angle between rotor and stator needs to be 90° . So, to achieve maximum, torque we need to make sure that there is a 90° difference between the opposing poles. We can do this by detecting the rotor angle. If we keep tracking the rotor angle, then we can supply voltage to the stator coils when the opposing poles are 90° apart from each other. An encoder attached to the motor can give us the rotor angle. So, if we provide a sinusoidal current input to the motor, the peak current should occur when the opposing poles will be 90° apart from each other.

However, the actual voltage that's being applied to each phase of the motor is equal to the voltage supplied minus the back emf. If the back emf and applied voltage are in phase with each other, then the resulting peak voltage (applied voltage minus the back emf) needs to occur when the opposing poles are 90° apart. But as the speed of the motor is increased, the back emf will start to become out of phase with the applied voltage. And when that happens, the resulting peak voltage will no longer occur at the 90° phase difference of the opposing poles. So, the amount of torque generated will be reduced. And it will continue to reduce with the increasing operating speed of the system. As torque is the driving force in the motor, this will result in a speed reduction of the motor. And if there is a controller being used to maintain the speed it will command more voltage to produce the required

torque which may not be achieved because of the saturation in the motor and we may not achieve our required speed.

2.1 Field Oriented Control

So, in order to have maximum torque the back emf and phase currents of the stator coils needs to be in phase. Therefore, field-oriented control (FOC) is used. Field-oriented control (FOC) is also known as vector control. FOC controls the phase currents. The FOC makes sure that the peak current will take place at a time that will lead to stator and rotor flux to be 90° away from each other. Currents in the motor phases are measured. And if the resultant current doesn't produce a stator flux that is 90° away from the rotor flux then based on the error signal a combination of phase currents is commanded that will create the required flux that will occur at 90° away from rotor flux.

Now, dealing with three sinusoidal currents can be complicated and the controller needs to be very fast to control such currents. Using the Clarke transformation, this complication can be minimized. The forward Clarke transformation changes the three sinusoidal phase currents (I_A, I_B, I_C) into two sinusoidal currents (I_α, I_β). The three-phase currents are converted into a 2-axis coordinate system from the 3-axis system of the stator. Here, I_α and I_β are stator currents converted into a two-phase system. But the coordinates of this two-phase system are still time-varying. And it's still a complex process to track them with a conventional controller. If these time-varying coordinates can be converted into time-invariant coordinates, then some complexity can be eliminated. This can be done by using the Park transformation. The park transformation converts two sinusoidal (I_α, I_β) currents into two dc (I_d, I_q) currents. I_d and I_q are direct and quadrature stator currents from the rotor perspective. I_d represents the current that will produce a magnetic flux that is in phase with

the rotor. So, we want this current to be zero so that this doesn't result in torque reduction. A PI controller will command a corrective signal flowing to the motor phases so that d-current remains zero and q-current achieves the required magnitude. The controller signal is then converted to α - β voltages using the inverse Park transformation. The α - β voltages are further converted to three phase voltages using the inverse Clarke transformation.

2.1.1 Clarke Transformation

If the phase currents are I_A , I_B , I_C , then the α - β currents can be given by, [6]

$$\begin{bmatrix} I_\alpha \\ I_\beta \end{bmatrix} = k \begin{bmatrix} 1 & -\frac{1}{2} & -\frac{1}{2} \\ 0 & \frac{\sqrt{3}}{2} & -\frac{\sqrt{3}}{2} \end{bmatrix} \begin{bmatrix} I_A \\ I_B \\ I_C \end{bmatrix} \quad (2.2)$$

$$I_{\alpha\beta} = kCI_{ABC}. \quad (2.3)$$

Here, k is a scaling factor. I_{ABC} is the phase current matrix. C is the forward Clarke transformation matrix and it converts the phase current matrix to $I_{\alpha\beta}$. To find the inverse Clarke transformation which will convert α - β currents back into phase currents we need to invert this equation.

$$I_{ABC} = \frac{1}{k} C^{-1} I_{\alpha\beta}. \quad (2.4)$$

Inverting matrix C we get [6],

$$\begin{bmatrix} I_A \\ I_B \\ I_C \end{bmatrix} = \frac{1}{k} \begin{bmatrix} \frac{2}{3} & 0 \\ -\frac{1}{3} & \frac{1}{\sqrt{3}} \\ -\frac{1}{3} & -\frac{1}{\sqrt{3}} \end{bmatrix} \begin{bmatrix} I_\alpha \\ I_\beta \end{bmatrix}. \quad (2.5)$$

So, here Clarke transformation is, $C = \begin{bmatrix} 1 & -\frac{1}{2} & -\frac{1}{2} \\ 0 & \frac{\sqrt{3}}{2} & -\frac{\sqrt{3}}{2} \end{bmatrix}$.

And, inverse Clarke transformation is, $C^{-1} = \begin{bmatrix} \frac{2}{3} & 0 \\ -\frac{1}{3} & \frac{1}{\sqrt{3}} \\ -\frac{1}{3} & -\frac{1}{\sqrt{3}} \end{bmatrix}$.

But these forms of Clarke transformations can be further simplified, which will be used later in this paper.

We know that summation of the phase currents is equal to zero. So, we can write the following equations.

$$\sum I = 0 \quad (2.6)$$

Or, $\frac{1}{2}I_A = -\frac{1}{2}I_B - \frac{1}{2}I_C.$ (2.7)

Now, from equation (2.2),

$$I_\alpha = k(I_A - \frac{1}{2}I_B - \frac{1}{2}I_C) \quad (2.8)$$

Or, $I_\alpha = k(I_A + \frac{1}{2}I_A)$ (2.9)

Or, $I_\alpha = k(\frac{3}{2}I_A + 0.I_B + 0.I_C).$ (2.10)

So, equation (2 .2) now becomes,

$$\begin{bmatrix} I_\alpha \\ I_\beta \end{bmatrix} = k \begin{bmatrix} \frac{3}{2} & 0 & 0 \\ 0 & \frac{\sqrt{3}}{2} & -\frac{\sqrt{3}}{2} \end{bmatrix} \begin{bmatrix} I_A \\ I_B \\ I_C \end{bmatrix}. \quad (2 .11)$$

Now, we can further write,

$$-\frac{\sqrt{3}}{2} I_C = \frac{\sqrt{3}}{2} I_A + \frac{\sqrt{3}}{2} I_B. \quad (2 .12)$$

From equation (2 .2),

$$I_\beta = \frac{\sqrt{3}}{2} I_B - \frac{\sqrt{3}}{2} I_C \quad (2 .13)$$

Or,

$$I_\beta = \frac{\sqrt{3}}{2} I_B + \frac{\sqrt{3}}{2} I_A + \frac{\sqrt{3}}{2} I_B. \quad (2 .14)$$

So,

$$I_\beta = \frac{\sqrt{3}}{2} I_A + \sqrt{3} I_B. \quad (2 .15)$$

So, equation (2 .11) now becomes,

$$\begin{bmatrix} I_\alpha \\ I_\beta \end{bmatrix} = k \begin{bmatrix} \frac{3}{2} & 0 & 0 \\ \frac{\sqrt{3}}{2} & \sqrt{3} & 0 \end{bmatrix} \begin{bmatrix} I_A \\ I_B \\ I_C \end{bmatrix}. \quad (2 .16)$$

Now, inverting equation (2 .16) [6],

$$\begin{bmatrix} I_A \\ I_B \\ I_C \end{bmatrix} = \frac{1}{k} \begin{bmatrix} \frac{2}{3} & 0 \\ -\frac{1}{3} & \frac{1}{\sqrt{3}} \\ 0 & 0 \end{bmatrix} \begin{bmatrix} I_\alpha \\ I_\beta \end{bmatrix}. \quad (2.17)$$

As can be seen, the phase current I_C cannot be directly determined from equation (2.17).

So, for the inverse transformation equation (2.5) will be used in this paper instead of equation (2.17).

So, the new form of forward and inverse Clark transformation matrices are,

$$C = \begin{bmatrix} \frac{3}{2} & 0 & 0 \\ \frac{\sqrt{3}}{2} & \sqrt{3} & 0 \end{bmatrix} \text{ and } C^{-1} = \begin{bmatrix} \frac{2}{3} & 0 \\ -\frac{1}{3} & \frac{1}{\sqrt{3}} \\ -\frac{1}{3} & -\frac{1}{\sqrt{3}} \end{bmatrix}.$$

This form of Clarke and inverse Clarke transformation matrices will be used in this paper.

In equation (2.16) and (2.17) k is a scaling factor. For this paper, the value of k is chosen to be $2/3$.

2.1.2 Park Transformation

The Park transformation converts two-time varying currents from α - β coordinates to stationary d-q frame currents. The inverse park transformation changes d-q currents into α - β currents. Time-invariant d-q currents are easier for the controller to track and control. If the currents in the α - β frame are I_α and I_β , currents in the d-q frame are I_d and I_q and the rotor angle is θ_r then forward Park transformation is [6]

$$\begin{bmatrix} I_d \\ I_q \end{bmatrix} = \begin{bmatrix} \cos(\theta_r) & \sin(\theta_r) \\ -\sin(\theta_r) & \cos(\theta_r) \end{bmatrix} \begin{bmatrix} I_\alpha \\ I_\beta \end{bmatrix} \quad (2.18)$$

Or,
$$I_{dq} = P I_{\alpha\beta} . \quad (2.19)$$

And the inverse park transformation is given by equation (2.20) [6].

$$\begin{bmatrix} I_\alpha \\ I_\beta \end{bmatrix} = \begin{bmatrix} \cos(\theta_r) & -\sin(\theta_r) \\ \sin(\theta_r) & \cos(\theta_r) \end{bmatrix} \begin{bmatrix} I_d \\ I_q \end{bmatrix} \quad (2.20)$$

$$I_{\alpha\beta} = P^{-1} I_{dq} . \quad (2.21)$$

The Park and inverse Park transformation matrices are,

$$P = \begin{bmatrix} \cos(\theta_r) & \sin(\theta_r) \\ -\sin(\theta_r) & \cos(\theta_r) \end{bmatrix} \text{ and } P^{-1} = \begin{bmatrix} \cos(\theta_r) & -\sin(\theta_r) \\ \sin(\theta_r) & \cos(\theta_r) \end{bmatrix} .$$

2.2 Uncontrolled Current Operation

In this method, the phase currents are not controlled, unlike the field-oriented control. This is why this method is much simpler than the FOC method. The voltage is supplied to the motor and we let the currents work on their own. The performance of the motor operating with this method would be flawless if the commutation of the motor is running perfectly. But, with increasing speeds, the back emf will start to become out of phase with the input voltage. As discussed before, this will cause the peak current not to occur in a position which will cause the opposing poles to be 90° apart from each other. However, this situation happens and continues to increase after a certain speed. Before that speed, the motor should work just fine. The speed at which the motor phase currents will start to become out of phase depends on the motor's electrical properties. Depending on the size and capacity of the motor it can vary. In this paper, we will experiment with uncontrolled current operation and discuss until when this method works just as good as FOC. If the

motor works fine without any current control and the back emf remains in phase with the current, then there is no point of implementing FOC. However, after a certain speed, when the back emf will start to become out of phase, the FOC becomes useful as it controls the current to generate the peak current at the required time. We will experiment with both of the method and see how useful really FOC is compared to the uncontrolled current operation. Looking at the bandwidths of two systems with these two methods implemented we can predict when there will be phase shifting. And depending on the application or requirement of the operating range we can decide which system will be more useful, considering both the cost and performance of the system.

Chapter 3 - Building Simulation

In chapter 3 we will discuss how Simulink simulations were built. In order to understand how the system behaves with the methods described in Chapter 2 , we need to run simulations. A simulation model can tell a lot about our system. We can learn from the simulation, given that we have considered and incorporated all the necessary system dynamics. Two simulation models will be needed as we need to simulate both FOC and uncontrolled current operation. We will discuss how different function blocks were built in those simulation models. Most of the blocks will be the same for both simulation models. The only difference that we will see is the simulation with vector control will implement FOC with several additional blocks and simulation with uncontrolled current operation will use a voltage divider block instead.

3.1 State Space Formulation of the Electrical Dynamics of the Motor

To define the electrical dynamics of the Brushless DC (BLDC) motor in the simulation we will use state space representation. Three phases of the BLDC motor take three voltages as inputs. The output of the electrical dynamics is three phase currents generated from the input voltages. As discussed before, the resulting input voltage in the motor phases is equal to the applied voltage minus the back emf. So, when formulating the state space, we need to consider this aspect as well.

Now, let's consider a BLDC motor with Y-connection, having three phases A, B and C as can be seen in Figure 3.1. The voltage inputs to the phases are V_a , V_b and V_c respectively. Back emf generated in those phases are V_{ae} , V_{be} and V_{ce} . The currents generated due to the resulting input voltage in the phases are I_a , I_b and I_c .

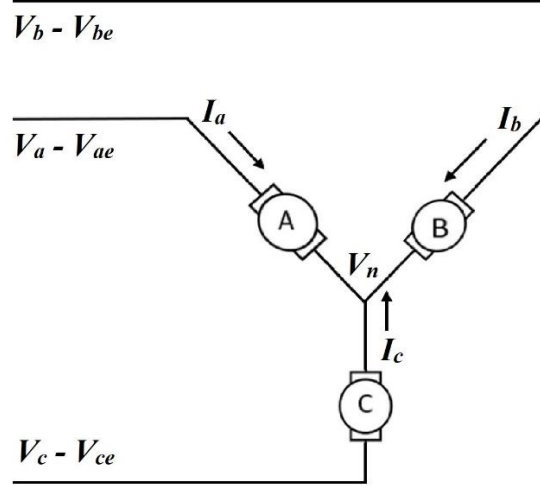


Figure 3.1: Schematic diagram of a BLDC Motor.

Now, we know that summation of the phase currents of a BLDC motor is equal to zero.

$$I_a + I_b + I_c = 0 \quad (3.1)$$

Or,
$$I_a = -(I_b + I_c) \quad (3.2)$$

Or,
$$I_b = -(I_a + I_c) \quad (3.3)$$

Or,
$$I_c = -(I_a + I_b) . \quad (3.4)$$

Differentiating equations (3.4) shows,

$$\dot{I}_c = -(\dot{I}_a + \dot{I}_b) . \quad (3.5)$$

Now, let's consider each phase of the motor has resistance R and inductance L. If the voltage at the point where all three phases meet is V_n , then From Kirchhoff's voltage law we can write,

$$V_a - V_{ae} - V_n = L\dot{I}_a + RI_a , \quad (3.6)$$

$$V_b - V_{be} - V_n = L\dot{I}_b + RI_b , \quad (3.7)$$

And,
$$V_c - V_{ce} - V_n = L\dot{I}_c + RI_c \quad (3.8)$$

Or,
$$V_n = -L\dot{I}_c - RI_c + (V_c - V_{ce}). \quad (3.9)$$

Using equation (3.5) we get

$$V_n = L(\dot{I}_a + \dot{I}_b) + R(I_a + I_b) + (V_c - V_{ce}). \quad (3.10)$$

From equation (3.6) we can write

$$(V_a - V_{ae}) - (V_c - V_{ce}) - L(\dot{I}_a + \dot{I}_b) - R(I_a + I_b) = L\dot{I}_a + RI_a \quad (3.11)$$

Or,
$$(V_a - V_{ae}) - (V_c - V_{ce}) = 2L\dot{I}_a + L\dot{I}_b + 2RI_a + RI_b. \quad (3.12)$$

Similarly, from equation (3.7) we can write,

$$(V_b - V_{be}) - (V_c - V_{ce}) = 2L\dot{I}_b + L\dot{I}_a + 2RI_b + RI_a. \quad (3.13)$$

By re-arranging we get the state equations of

$$2L\dot{I}_a + L\dot{I}_b = -2RI_a - RI_b + (V_a - V_{ae}) - (V_c - V_{ce}) \quad (3.14)$$

And,
$$2L\dot{I}_b + L\dot{I}_a = -2RI_b - RI_a + (V_b - V_{be}) - (V_c - V_{ce}) \quad (3.15)$$

Where,
$$I_c = -(I_a + I_b). \quad (3.16)$$

Here I_a, I_b are the state variables. Having only two state variables, it is less cumbersome.

However, phase current I_c can be easily determined using equation (3.16). From these

equations, the state space and output equations are

$$\begin{bmatrix} 2L & L \\ L & 2L \end{bmatrix} \begin{bmatrix} \dot{I}_a \\ \dot{I}_b \end{bmatrix} = \begin{bmatrix} -2R & -R \\ -R & -2R \end{bmatrix} \begin{bmatrix} I_a \\ I_b \end{bmatrix} + \begin{bmatrix} 1 & 0 & -1 \\ 0 & 1 & -1 \end{bmatrix} \begin{bmatrix} V_a - V_{ae} \\ V_b - V_{be} \\ V_c - V_{ce} \end{bmatrix} \quad (3.17)$$

$$\begin{bmatrix} \dot{I}_a \\ \dot{I}_b \end{bmatrix} = \begin{bmatrix} 2L & L \\ L & 2L \end{bmatrix}^{-1} \begin{bmatrix} -2R & -R \\ -R & -2R \end{bmatrix} \begin{bmatrix} I_a \\ I_b \end{bmatrix} + \begin{bmatrix} 2L & L \\ L & 2L \end{bmatrix}^{-1} \begin{bmatrix} 1 & 0 & -1 \\ 0 & 1 & -1 \end{bmatrix} \begin{bmatrix} V_a - V_{ae} \\ V_b - V_{be} \\ V_c - V_{ce} \end{bmatrix} \quad (3.18)$$

$$Y = I = \begin{bmatrix} I_a \\ I_b \\ I_c \end{bmatrix} = \begin{bmatrix} 1 & 0 \\ 0 & 1 \\ -1 & -1 \end{bmatrix} \begin{bmatrix} I_a \\ I_b \end{bmatrix}. \quad (3.19)$$

Here, equation (3.18) is the state space equation and equation (3.19) is the output equation.

From equation (3.18) and (3.19) we defined the state space matrices:

$$\text{State matrix, } A = \begin{bmatrix} 2L & L \\ L & 2L \end{bmatrix}^{-1} \begin{bmatrix} -2R & -R \\ -R & -2R \end{bmatrix}$$

$$\text{Input matrix, } B = \begin{bmatrix} 2L & L \\ L & 2L \end{bmatrix}^{-1} \begin{bmatrix} 1 & 0 & -1 \\ 0 & 1 & -1 \end{bmatrix}$$

$$\text{Output matrix, } C = \begin{bmatrix} 1 & 0 \\ 0 & 1 \\ -1 & -1 \end{bmatrix}$$

$$\text{Feed through matrix, } D = \begin{bmatrix} 0 \\ 0 \\ 0 \end{bmatrix}$$

These matrices will be used in the state space block of the Simulink simulation to define our motor.

3.2 Torque Production from Sinusoidal Currents

The amount of torque produced by a motor is directly related to the amount of current flowing through the phases. In case of a brushed dc motor, if the motor torque constant is k_t , the current flowing through the motor is I , then the torque T produced is

$$T = k_t I . \quad (3 .20)$$

Instead of k_t we could also use the back emf constant k_b . Because, for a motor, the torque constant k_t is the same as the back emf constant k_b [6]. However, for a 3-phase BLDC motor, it's not as simple as a brushed dc motor. The torque that's being generated in a BLDC motor is the resultant of torque generation in each phase. And with sinusoidal current input, the amount of torque generated in each phase varies with time. But the resultant torque remains more or less constant because of the varying torque production in different phases. The average torque generation can be predicted if we know the peak magnitude of the instantaneous current.

If per phase back emf constant of the motor is given by k_b , the angular displacement of the rotor is θ_r and currents in the three phases are I_a , I_b , and I_c then the constant torque output T is [6]

$$T = -k_b \sin(\theta_r)I_a - k_b \sin(\theta_r + 120^\circ)I_b - k_b \sin(\theta_r - 120^\circ)I_c . \quad (3 .21)$$

If sinusoidal currents of amplitude I_p are supplied to all the windings and they are in phase with the back emf the torque produced is given by the equation (3 .24) ,

$$\begin{aligned} T = & [-k_b \sin(\theta_r)][-I_p \sin(\theta_r)] + [-k_b \sin(\theta_r - 120^\circ)][-I_p \sin(\theta_r - 120^\circ)] \\ & + [-k_b \sin(\theta_r + 120^\circ)][-I_p \sin(\theta_r + 120^\circ)] \end{aligned} \quad (3 .22)$$

$$\text{Or,} \quad T = k_b I_p [\sin^2 \theta_r + \sin^2(\theta_r - 120^\circ) + \sin^2(\theta_r + 120^\circ)] \quad (3 .23)$$

Or,
$$T = \frac{3}{2} k_b I_p. \quad (3.24)$$

Each phase differs from each other by 120° , contributes a \sin^2 term that result in a constant torque output as shown in Figure 3.2. [6].

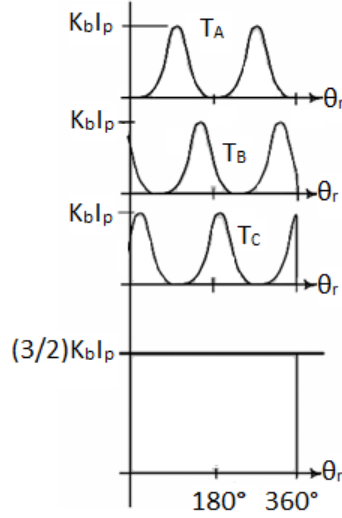


Figure 3.2: Torque production in sinusoidal BLDC motor.

Thus, when the phase currents are in phase with the back EMF the torque produced is proportional to the peak current. And the torque produced in the motor is 1.5 times larger than the torque produced in the phase with peak current I_p . This is the maximum torque generated in the motor with perfect commutation.

In the simulation, a block will be added which will take the phase currents as input and will produce torque as output. Equation (3.21) will be used to convert the phase currents into torque. Although much simpler, equation (3.24) will not be used in the torque production block of the simulation because the outputs are sinusoidal currents. Using equation (3.21), the block will be able to accurately generate the torque. However, equation (3.24) can be used to predict the torque generated in ideal condition (i.e. when currents and back emf are

in phase with each other). If the torque generated in the output of the torque block in simulation doesn't match with the torque calculated using equation (3.24) (by taking the peak current from state space output), we can predict phase shifting in the back emf generated with the phase currents. Or, in other words, if the factor is not $3/2$ for motor torque generated from peak current, then we can accurately predict commutation is not ideal and phase currents and back emf are out of phase. This technique will be discussed in the later chapters to compare FOC with uncontrolled current operation predicting until when commutation in both systems works perfectly.

3.3 Motor Mechanical Plant

Although the commutation, torque generation all happens together inside the motor and mechanical speed is an output of the motor, for simulation purpose we break them down into different blocks to keep our model of the system simple. In this section, we will discuss the mechanical plant of the system, specifically the speed model of the motor. This block of the simulation takes torque as input and generates speed as the output.

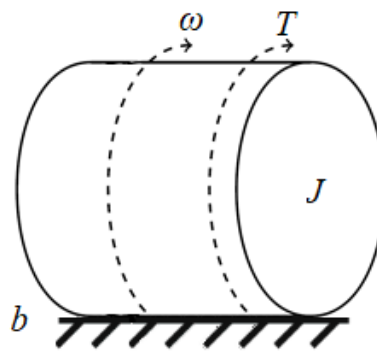


Figure 3.3: Speed model of the motor.

Let us consider the friction of our motor is viscous, and the friction coefficient is b as shown in Figure 3.3. Now, if the moment of inertia of the motor is J , the speed of the motor is given by ω , then torque T is given by

$$T(t) = J\dot{\omega}(t) + b\omega(t) \quad (3.25)$$

Taking the Laplace transform of equation (3.25) and considering zero initial speed of the motor we get the following s-domain

$$T(s) = (Js + b)\omega(s) \quad (3.26)$$

$$\frac{\omega(s)}{T(s)} = \frac{1}{Js + b} \quad (3.27)$$

The transfer function in equation (3.27) will be used to generate the angular speed of the motor from torque in the mechanical plant function block of the Simulink simulation.

3.4 Vector Control

This section is only applicable to the simulation model with vector control. The vector control or FOC method will be implemented using several blocks. We will be using individual blocks for forward Clarke, forward Park, inverse Clarke and inverse Park transformations. The forward Clarke transformation will take the output of the state space block or the phase currents as input. The output of the Clarke transformation will be used as input for the Park transformation. The Park transformation block also takes the rotor electrical position as input. The Park transformation provides dc d-q currents. We want the d current to be zero and the q current to be a required constant value. For this purpose, two PI controller block will be used, one for each current, to maintain these required values. The output of the controllers will be the corrective voltage signals in the d-q reference frame. These voltages will then be converted to α - β voltages using an inverse Park

transformation block and rotor electrical position. The α - β voltages will be converted to three sinusoidal voltages as the input voltage for the motor phases using an inverse Clarke transformation block. Equations (2 .16) and (2 .5) will be used in the forward and inverse Clarke transformation function blocks respectively. Equations (2 .18) and (2 .20) will be used in the forward and inverse Park transformation function blocks, respectively.

3.5 Voltage Synchronizer

This section only applies to the simulation model with the uncontrolled current operation. The three phases of the BLDC motor take three voltage inputs. However, we want to command a scalar voltage input that will be necessary to get our required speed. The voltage divider takes that scalar voltage and divides it to three outputs using the angular electrical position of the rotor, which then is used as the inputs for the three phases of the motor. This is especially helpful to simulate the operation when we are using a controller for the motor speed. The controller takes the speed error of the motor and generates a single voltage command as the correction signal based on the error signal. The voltage divider function block then produces three input voltages for the three phases from the controller output voltage. This way we keep our simulation block simple and free from complexity. Now, if the average voltage command from the controller is V_c and the rotor angle is θ_r , then V_c can be divided into three voltages using

$$V = \begin{bmatrix} V_a \\ V_b \\ V_c \end{bmatrix} = \begin{bmatrix} -V_c \sin(\theta_r) \\ -V_c \sin(\theta_r - 120^\circ) \\ -V_c \sin(\theta_r + 120^\circ) \end{bmatrix} \quad (3.28)$$

This equation will be used in the voltage divider function block of the simulation model with the uncontrolled current operation.

3.6 Back EMF

Like commutation, electrical dynamics and torque generation, back emf is also produced inside of the motor. But as mentioned before, to simulate our system we break down these into individuals blocks to avoid complexity. The back emf is directly related to the electrical speed of the rotor. This is why the back emf function block takes the electrical speed of the rotor as input. The electrical speed multiplied with the back emf constant of the motor gives us the back emf. Now, the back emf generated reduces the input voltages to the motor phases. So, we need three back emf that will be varying with time for three different phases. The amount of back emf that will be generated in a phase depends on the rotor position of the motor. So, the back emf block also takes the rotor electrical position as input. Thus, using rotor electric position and speed the back emf block produces three different back emf signal for three motor phases. The back emf voltages are subtracted from the input voltages and the resultant voltages are fed to the state space block as inputs. Now, if the electrical speed of the rotor is ω_e , the electrical rotor position is θ_r and per phase back emf constant of the motor is k_b , then the back emf for three phases can be found from equation (3 .29). This equation will be used in the back emf function block of the simulation.

$$V_{bemf} = \begin{bmatrix} V_{ae} \\ V_{be} \\ V_{ce} \end{bmatrix} = \begin{bmatrix} -\omega_e k_b \sin(\theta_r) \\ -\omega_e k_b \sin(\theta_r - 120^\circ) \\ -\omega_e k_b \sin(\theta_r + 120^\circ) \end{bmatrix}. \quad (3 .29)$$

3.7 Simulation Models

As discussed earlier, we will use two separate simulation models for a speed control system with vector control and system with the uncontrolled current operation. We will also have two simulation models for a position control system. The speed control simulation model for a system with vector control is shown in Figure 3.4. And the simulation model for the speed control system with the uncontrolled current operation is shown in Figure 3.5. The simulation model for a position control is shown in Figure 3.6 and Figure 3.7 for vector control and the uncontrolled current, respectively. In these simulation models, we have used various variables that must be defined in the MATLAB workspace prior to running the simulations. A MATLAB code, named `initialization.m` is written which will create all the necessary variables and calculations needed for the simulations in the workspace. This code must be run before running any of the simulation models. The `initialization.m` can be found in Appendix A. MATLAB codes used to define different function blocks in the simulation models also can be found in Appendix A. Notice no delays are added to the simulation models, because we are assuming the system is ideal at this point and the computer that performs all the necessary calculations and controlling is infinitely fast. We will consider and add the necessary delays to the simulation in the later chapters. The delays may be present in a realistic system.

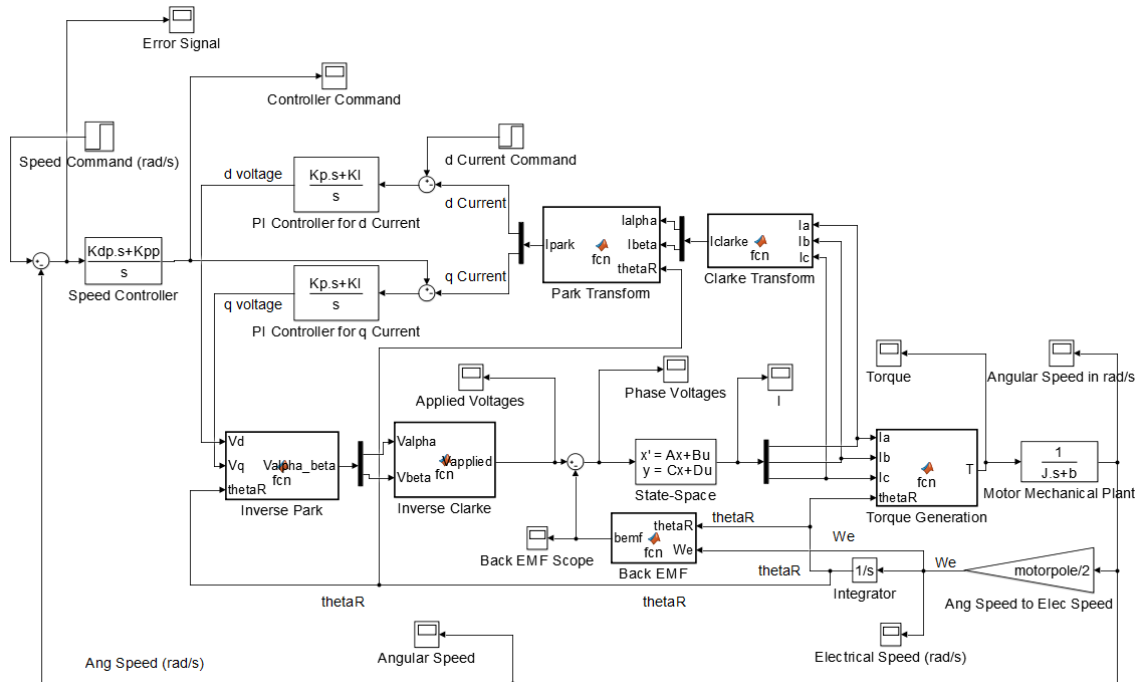


Figure 3.4: Simulation Model for Speed Control System with Vector Control Operation.

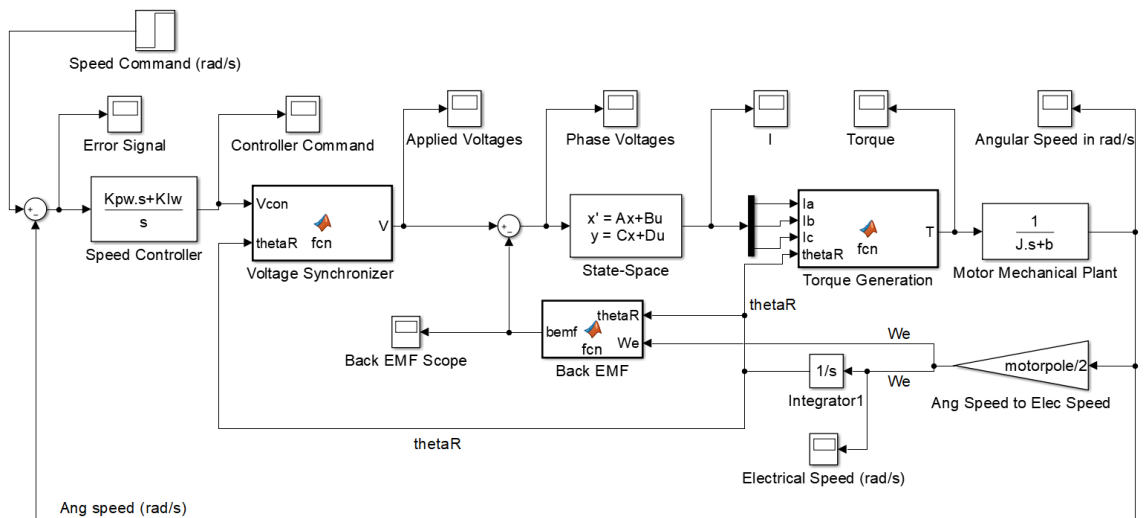


Figure 3.5: Simulation Model for Speed Control System with Uncontrolled Current Operation.

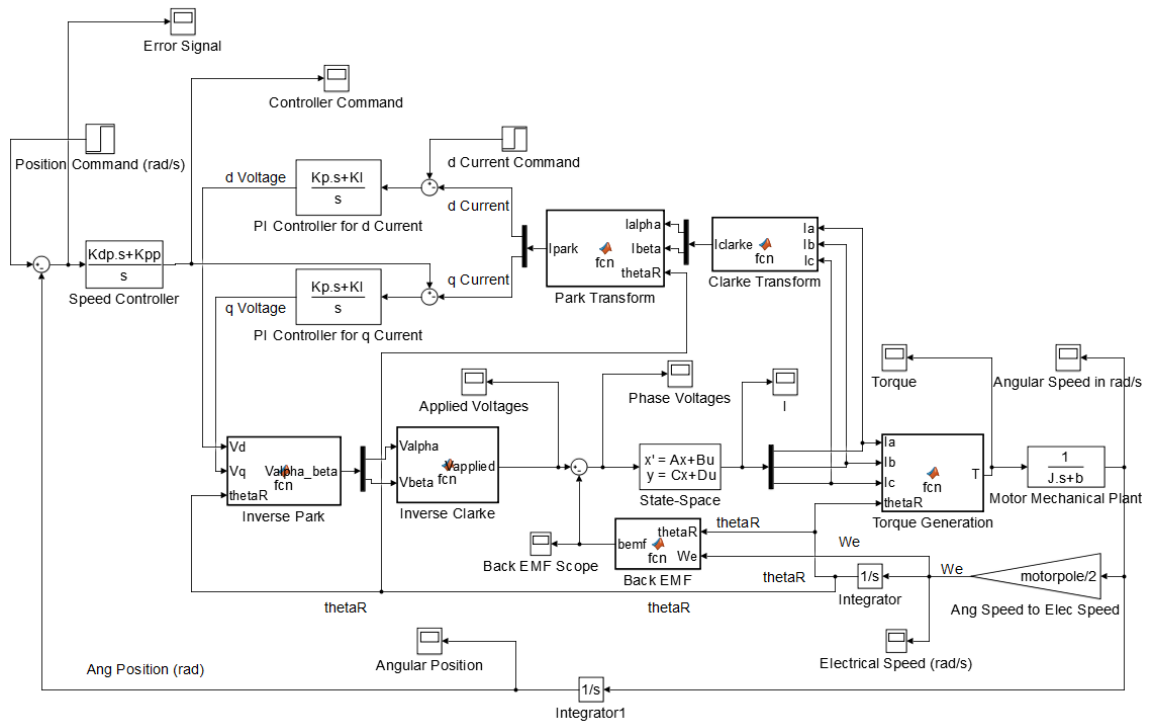


Figure 3.6: Simulation Model for Position Control System with Vector Control Operation.

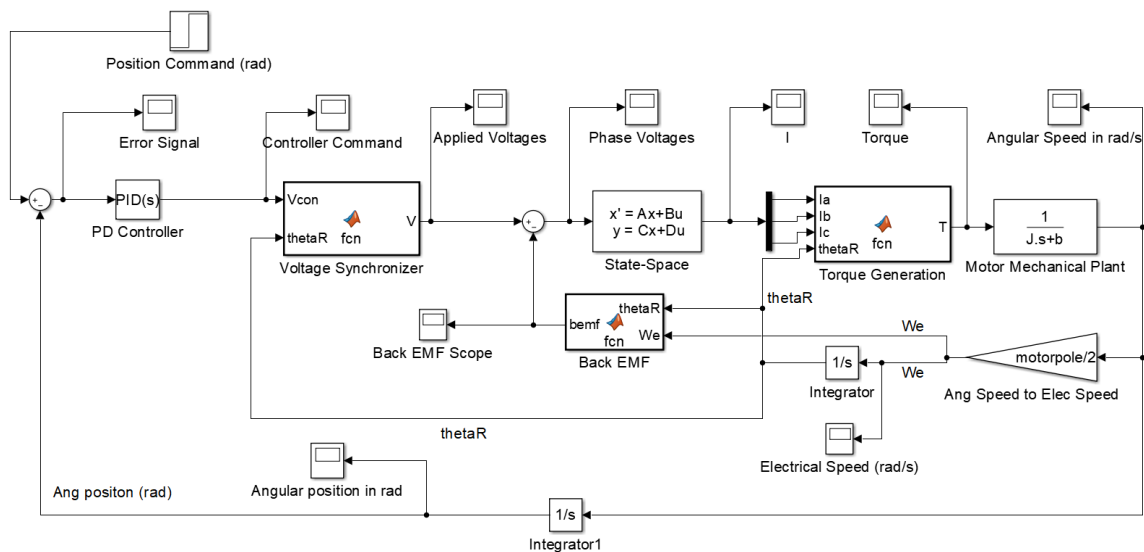


Figure 3.7: Simulation Model for Position Control System with Uncontrolled Current Operation.

Now, let's run the simulation model for speed control for both of the methods with a step input of 200 rad/s to observe the response. A PI controller with K_P as 10 and K_I as 100 was used to control the speed for both of the models. Other motor parameters such as the motor pole, the moment of inertia, friction coefficient, resistance and inductance etc. are chosen from an arbitrary motor. The chosen values can be found in the initialization.m code in Appendix A. From the system with vector control we get the angular speed response of the motor as shown in Figure 3.8. And, from the system with the uncontrolled current we get the angular speed response of the motor as shown in Figure 3.9. As can be seen from Figure 3.8 and Figure 3.9, the response of the system with vector control is slightly better than that of the system with uncontrolled current. For both of the systems, the speed reaches the steady-state speed of 200 rad/s as commanded. But for the system with vector control, the motor reaches the steady-state speed faster. In later chapters, we will discuss various situations in which the motor may need to run and continue to learn from the simulation models.

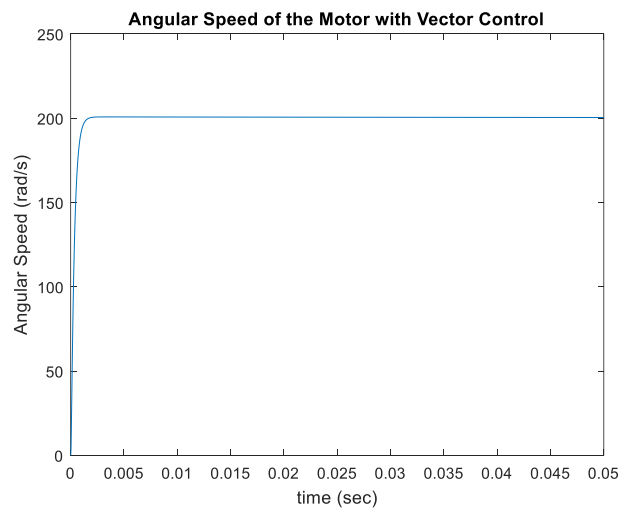


Figure 3.8: Angular Speed of the Motor with Vector Control.

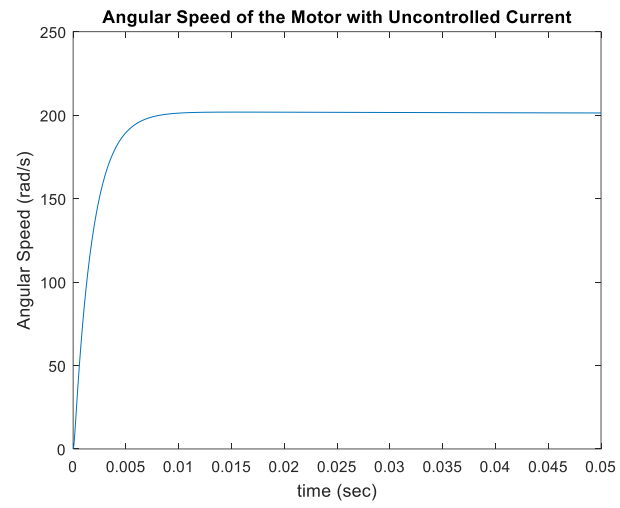


Figure 3.9: Angular Speed of the Motor with Uncontrolled Current.

Chapter 4 - Modeling and Frequency Response Analysis

In chapter 4 we will discuss modeling and frequency response of a system with Brushless DC (BLDC) motor for different applications with field-oriented control or vector control operation and uncontrolled current operation. We will generate the transfer function for the overall system to perform frequency response analysis. The aim is to understand how the operating range and the stability margins of the system vary with the two methods mentioned. To use these methods in actual hardware and decide which one has some advantage over the other one or which one gives better performance, we need to study the systems with these methods first. The frequency response of a system is an important aspect and it is, therefore, worth studying for the systems with the methods mentioned.

With that in mind, we will model the system implementing these methods in a BLDC motor. We will use the same motor from Chapter 3 as described in section 3.7 Simulation Models. We will perform modeling for the speed control systems and position control systems. Using these models, we can generate Bode plots for the of the systems mentioned. From the magnitude of the closed loop Bode plot, we can predict the bandwidth for these systems. Also, the phase plot can be useful to see if the output of a system is in phase with the input, which is important for better tracking and stability of the system. So, from this study, we can predict what operating speed range a system will track the command and at what speed the system will no longer be able to track the input.

4.1 Speed Control Model with Vector Control

We model the motor implementing vector control to generate speed with just one phase of the motor. The speed is controlled by a PI controller named G_{cw} . A different PI controller named G_{ci} is used to implement the vector control method. The torque constant of the motor is k_t and back emf constant is k_b . The motor has a moment of inertia of J and a friction coefficient of b . The electrical resistance of the stator windings is given by R and inductance is L . The speed command is ω_c and the measured speed is ω . Current command from the speed controller is I_c and the measured current produced by the motor electrical phases are I . The voltage command from the current controller is V_c . We assume that the commutation of the BLDC motor is perfect. Therefore, the electrical dynamics of the motor can be represented by transfer function G_{elec} and the mechanical dynamics is G_{mech} . We also assume that our system has unit feedback or the speed sensing system has a gain of one. The block diagram of the system for speed control with vector control is shown in Figure 4.1.

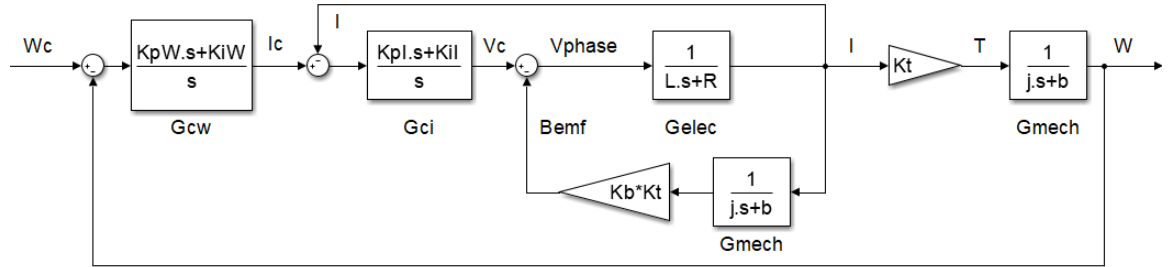


Figure 4.1: Speed control of a BLDC motor with vector control.

From Figure 4.1 we can write

$$G_{motor} = \frac{I}{V_c} = \frac{G_{elec}}{1 + k_b k_t G_{mech} G_{elec}}. \quad (4.1)$$

Vector control implemented is

$$G_{vec} = \frac{I}{I_c} = \frac{G_{motor} \cdot G_{ci}}{1 + G_{motor} \cdot G_{ci}}. \quad (4.2)$$

So, we can define the open loop transfer function as

$$(OL)_{vec} = G_{cw} G_{vec} k_t G_{mech}. \quad (4.3)$$

The closed loop speed control transfer function is

$$\left(\frac{\omega}{\omega_c}\right)_{vec} = \frac{(OL)_{vec}}{1 + (OL)_{vec}}. \quad (4.4)$$

Now, after substitute for all the transfer functions and simplifying we get

$$\begin{aligned} \left(\frac{\omega}{\omega_c}\right)_{vec} = & (K_p I K_{pW} k_t s^2 + K_{pW} K_{il} k_t s + K_{pl} K_{iW} k_t s + K_{iW} K_{il} k_t) / \\ & (LJ s^4 + (K_{pl} J + Lb + Rj) s^3 + (K_{pl} K_{pW} k_t + k_b k_t + K_{il} J + \\ & K_{pl} b + Rb) s^2 + (K_{il} K_{pW} k_t + K_{iW} K_{pl} k_t + K_{il} B) s + K_{il} K_{iW} k_t) \end{aligned} \quad (4.5)$$

4.2 Speed Control Model with Uncontrolled Current

In this section, we model the system to generate speed without implementing the vector control or in other words we model the system with the uncontrolled current input to the motor. Like section 4.1, we will use a PI controller to control the speed. For the most part, the block diagram is similar to what we saw in Figure 4.1. The only difference that we see is there is no controller for the current for implementing the vector control. So, the output of the controller now is the voltage command V_c for the motor. The other parameters of the motor and system characteristics remain the same as that of section 4.1 Speed Control Model with Vector Control. The block diagram of the speed control system with uncontrolled current is shown in Figure 4.2.

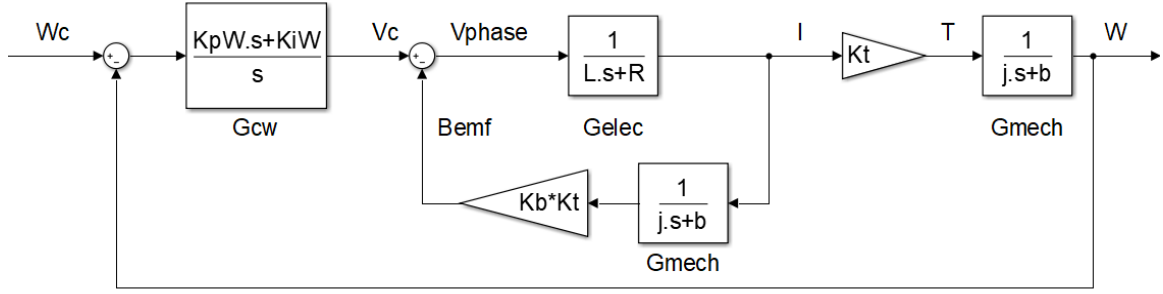


Figure 4.2: Speed control of a BLDC motor with uncontrolled current.

From Figure 4.2 we can write

$$G_{motor} = \frac{I}{V_c} = \frac{G_{elec}}{1 + k_b k_t G_{mech} G_{elec}}. \quad (4.6)$$

So, we can define the open loop transfer function for the system with uncontrolled current as,

$$(OL)_{uc} = G_{cw} G_{motor} k_t G_{mech}. \quad (4.7)$$

And, the closed loop speed control transfer function is given as,

$$\left(\frac{\omega}{\omega_c}\right)_{uc} = \frac{(OL)_{uc}}{1 + (OL)_{uc}}. \quad (4.8)$$

After substitute for all the transfer functions and simplifying we get,

$$\left(\frac{\omega}{\omega_c}\right)_{uc} = \frac{K_{pW} k_t s + K_{iW} k_t}{LJs^3 + (Lb + RJ)s^2 + (k_b k_t + K_{pW} k_t + Rb)s + K_{iW} k_t}. \quad (4.9)$$

4.3 Position Control Model with Vector Control

In this section, we will model our system to generate the position of the motor with vector control implemented. The block diagram of this system is also almost the same as that of section 4.1 Speed Control Model with Vector Control. In section 4.1 Speed Control Model

with Vector Control, we modeled our system to produce motor speed. In this section, the same block diagram is used to generate the angular speed of the motor. The speed is then integrated to produce the position of the rotor shaft. All the motor parameters and system characteristics remain the same as that in section 4.1 Speed Control Model with Vector Control. The block diagram of the system to simulate the position control of the motor with vector control implemented is shown in Figure 4.3.

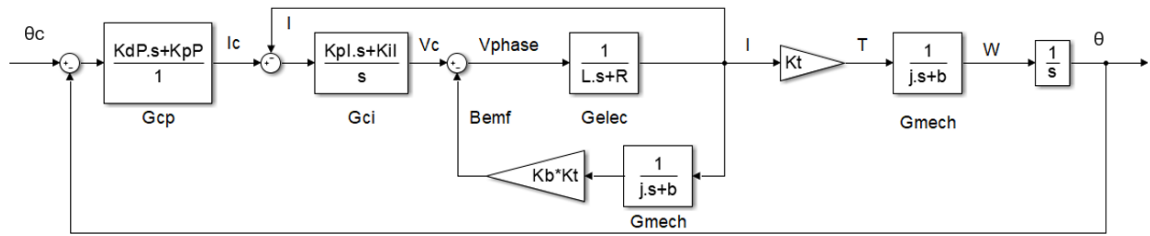


Figure 4.3: Position control of a BLDC motor with vector control.

From Figure 4.3 we can write

$$G_{motor} = \frac{I}{V_c} = \frac{G_{elec}}{1 + k_b k_t G_{mech} G_{elec}}. \quad (4.10)$$

Vector control is implemented as

$$G_{vec} = \frac{I}{I_c} = \frac{G_{motor} G_{ci}}{1 + G_{motor} G_{ci}}. \quad (4.11)$$

So, we can define the open loop transfer function as

$$(OL)_{vec} = G_{cp} G_{vec} k_t G_{mech} \frac{1}{s}. \quad (4.12)$$

The closed loop position control transfer function with vector control is given as

$$\left(\frac{\theta}{\theta_c}\right)_{vec} = \frac{(OL)_{vec}}{1 + (OL)_{vec}}. \quad (4.13)$$

After substitute for all the transfer functions and simplifying we get,

$$\begin{aligned}
\left(\frac{\theta}{\theta_c}\right)_{vec} = & (K_{dp}K_{pl}k_t s^2 + (K_{pp}K_{pl}k_t + K_{dp}K_{il}k_t)s + K_{pp}K_{il}k_t) / \\
& (LJs^4 + (K_{pl}J + Lb + RJ)s^3 + (K_{pl}K_{dp}k_t + k_b k_t + K_{il}J + \\
& K_{pl}b + Rb)s^2 + (K_{il}K_{dp}k_t + K_{pp}K_{pl}k_t + K_{il}b)s + K_{il}K_{pp}k_t)
\end{aligned} \quad (4.14)$$

4.4 Position Control Model with Uncontrolled Current

To generate the angular position of the motor using the uncontrolled current method we will use the same block diagram shown in Figure 4.2. But Figure 4.2 produces the angular speed of the motor. So, we need to integrate the angular speed to get the position. We assume the commutation of the motor is perfect and all the characteristics discussed previously remains the same. The block diagram for the position control system of the motor with the uncontrolled current operation is shown in Figure 4.4.

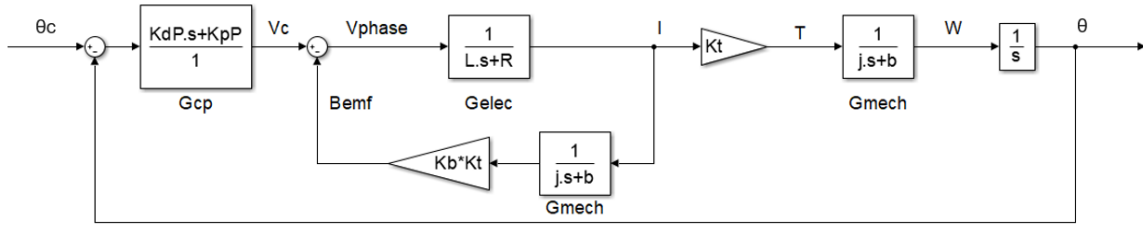


Figure 4.4: Position control of a BLDC motor with uncontrolled current.

Like before, from Figure 4.4 we can write

$$G_{motor} = \frac{I}{V_c} = \frac{G_{elec}}{1 + k_b k_t G_{mech} G_{elec}}. \quad (4.15)$$

Now, we can define the open loop transfer function as

$$(OL)_{uc} = G_{cp} G_{motor} k_t G_{mech} \frac{1}{s}. \quad (4.16)$$

So, the closed loop position control transfer function for the system with uncontrolled current is given as

$$\left(\frac{\theta}{\theta_c}\right)_{uc} = \frac{(OL)_{uc}}{1+(OL)_{uc}}. \quad (4.17)$$

After substitute for all the transfer functions and simplifying we get

$$\left(\frac{\theta}{\theta_c}\right)_{uc} = \frac{K_{dP}k_t s + K_{pP}k_t}{LJs^3 + (Lb + RJ)s^2 + (k_b k_t + K_{dP}k_t + Rb)s + K_{pP}k_t}. \quad (4.18)$$

4.5 Frequency Response of the Systems

Using the models in section 4.1, 4.2, 4.3 and 4.4 we can now generate Bode plots and perform frequency response analysis of the systems. The aim is to compare frequency responses of the systems with Field Oriented Control and Uncontrolled Current. Using the open loop transfer functions, we can generate open loop Bode plots. And using closed loop transfer functions we can generate closed-loop Bode plots. From the open loop Bode plots, we will be able to see the stability margins for these systems and can have an idea which system has better stability. And from the closed loop Bode plots, we can see the bandwidth of the systems and decide which system has a better operating frequency range and therefore can be run faster. We choose a PI controller for the vector control with K_p of 10 and K_i of 100. We will use this same current controller for systems described in section 4.1 and 4.3, the speed and position control system, respectively, with vector control. We also choose an arbitrary PI speed controller with K_{pw} of 10 and K_{iw} of 100. We will use this same speed controller for the systems in section 4.1 and 4.2, speed control system with vector control and uncontrolled current respectively. A PD position controller with K_{pp} of 10 and K_{dp} of 0.001 is chosen arbitrarily. This position controller will be used for the

systems in section 4.3 and 4.4, position control systems with vector control and uncontrolled current, respectively. We are using the same controller. So, that everything in the systems remains similar and we can compare the performance of the systems solely based on the vector control and uncontrolled current operation. The MATLAB code that generates these Bode plots can be found in Appendix A under the name ‘Bode Plot Generator for Section 4.5’.

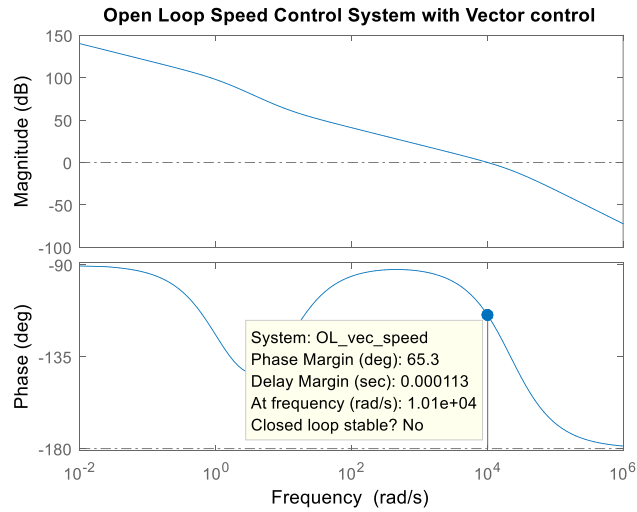


Figure 4.5: Open Loop Bode Plot of Speed Control System with Vector Control.

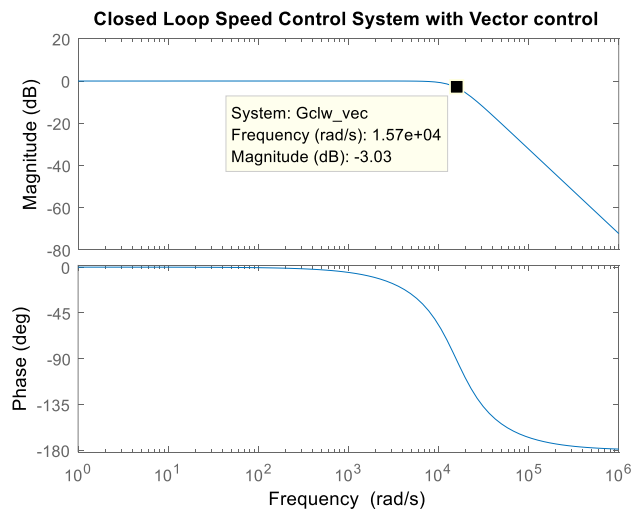


Figure 4.6: Closed Loop Bode Plot of Speed Control System with Vector Control.

From Figure 4.5 we can see the stability margin for the speed control system with vector control. And from Figure 4.6 we can see the closed-loop bandwidth of this system.

However, the phase margin of the system can be improved if we use a different current controller. For example, if we use a current controller with $K_p = 100$ and $K_i = 1000$ we get the frequency response as shown in Figure 4.7 and Figure 4.8. We can see that both bandwidth and phase margin is improved. However, the delay margin is significantly reduced and from the simulation, it is seen that this causes the system to go unstable when any delay is added. Now, if we reduce the gains to $K_p = 1$ and $K_i = 10$ we also get a better phase margin with big delay margin as shown in Figure 4.9. But with these reduced gains the closed loop bandwidth is also reduced significantly as shown in Figure 4.10. Also, in the lower frequency region, the phase plot almost drops to -180° which makes the system less stable in the lower speed. So, $K_p = 10$ and $K_i = 100$ is a good combination of gains for the current controller. And we will treat Figure 4.5 and Figure 4.6 as the frequency response for our speed control system with vector control.

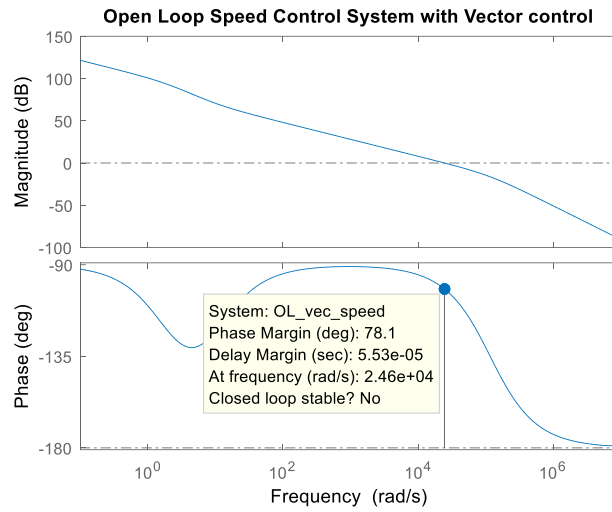


Figure 4.7: Open Loop Bode Plot of Speed Control System with Vector Control with $K_p = 100$ Amp/rad and $K_i = 1000$ Amp/rad/sec.

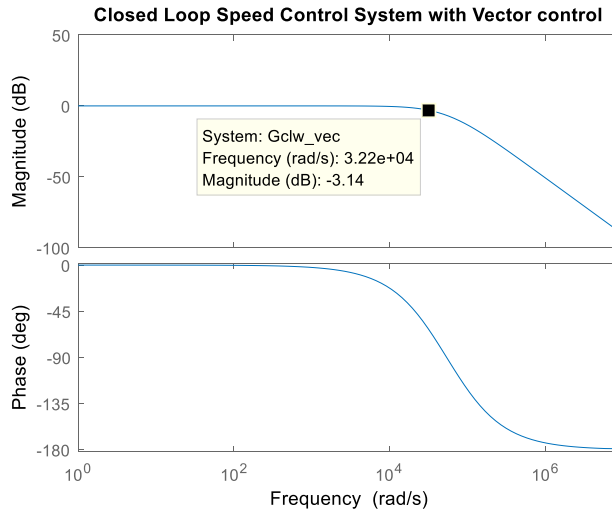


Figure 4.8: Closed Loop Bode Plot of Speed Control System with Vector Control with $K_p = 100$ Amp/rad and $K_i = 1000$ Amp/rad/sec.

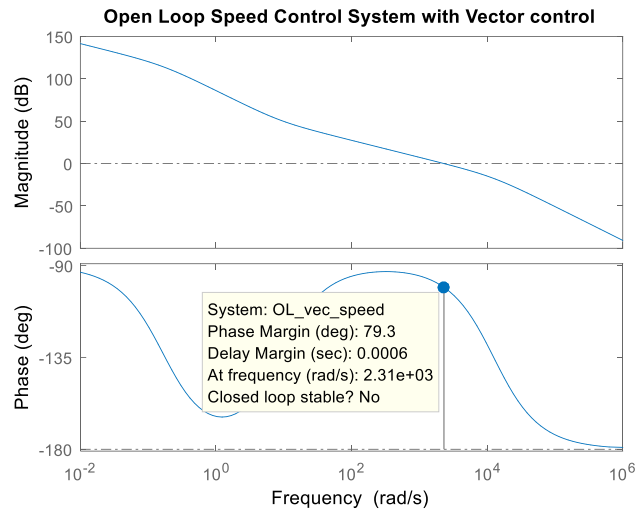


Figure 4.9: Open Loop Bode Plot of Speed Control System with Vector Control with $K_p = 1$ Amp/rad and $K_i = 10$ Amp/rad/sec.

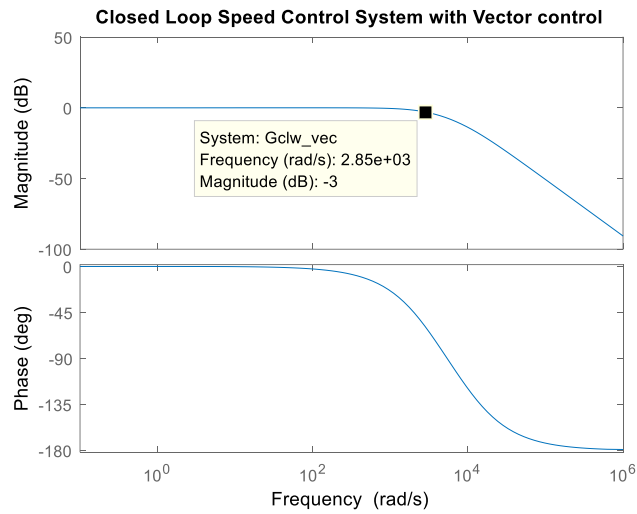


Figure 4.10: Closed Loop Bode Plot of Speed Control System with Vector Control with $K_p = 1$ Amp/rad and $K_i = 10$ Amp/rad/sec.

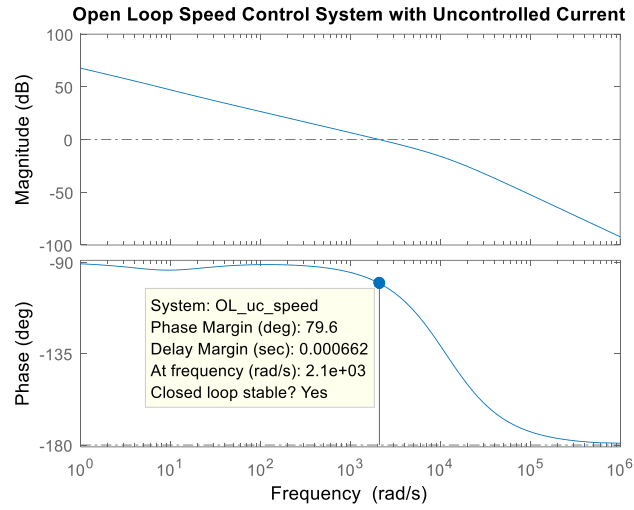


Figure 4.11: Open Loop Bode Plot of Speed Control System with Uncontrolled Current.

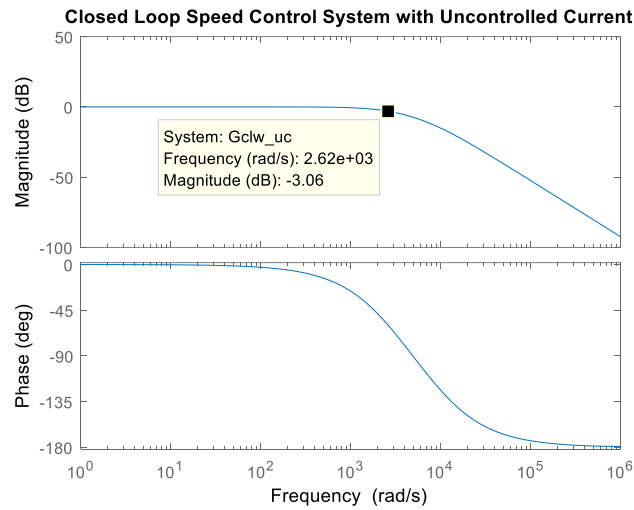


Figure 4.12: Closed Loop Bode Plot of Speed Control System with Uncontrolled Current.

As discussed, we will now compare Figure 4.5 with Figure 4.11 and Figure 4.6 with Figure 4.12. From the closed loop Bode plots, we see that the closed loop bandwidth of the speed control system with vector control is higher than that of the system with uncontrolled current. On the other hand, from the open loop Bode plots, we can see that the phase margin

of the same speed control system with vector control is lower than that of the system with uncontrolled current. So, it's clear that using vector control we can make the overall system faster but with the uncontrolled current we will have better stability. And having a better phase margin indicates that with uncontrolled current system there is more room for computer-generated delays and other dynamics that may not be considered in the model.

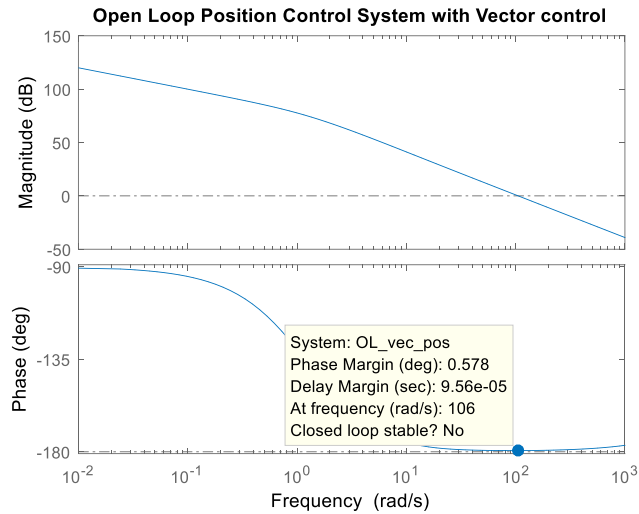


Figure 4.13: Open Loop Bode Plot of Position Control System with Vector Control.

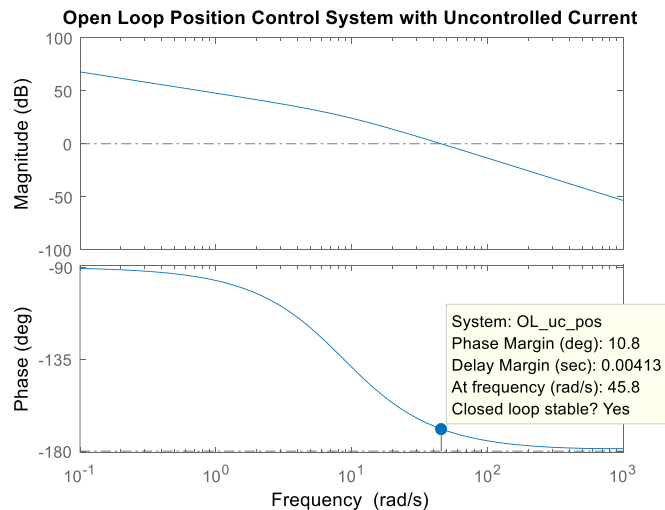


Figure 4.14: Open Loop Bode Plot of Position Control System with Uncontrolled Current.

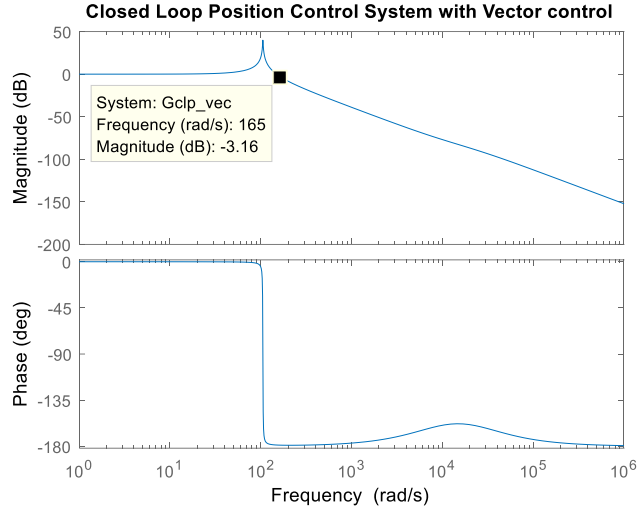


Figure 4.15: Closed Loop Bode Plot of Position Control System with Vector Control.

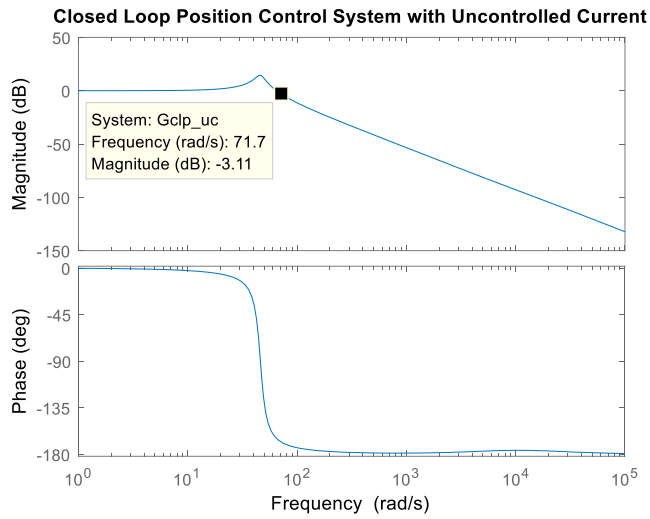


Figure 4.16: Closed Loop Bode Plot of Position Control System with Uncontrolled Current.

For position control, we also see from the closed loop Bode plots that, the closed loop bandwidth of the system with vector control is higher than that of the system with uncontrolled current. And also, from the open loop Bode plots, the phase margin of the

position control system with vector control is lower than that of the system with uncontrolled current.

Chapter 5 - Commutation

While modeling the motor in Chapter 4 we assumed the commutation of the BLDC motor is perfect. But in application it may not be the case always. Especially when the speed of the motor is high it is difficult to track the speed of the motor accurately and control the commutation accordingly. And also, depending on the speed of the controller itself the commutation of the motor may not be accurate at high speeds. When the commutation is not accurate it can affect the performance of the system. Therefore, it is important to discuss the commutation of the motor. In this chapter, we will analyze the commutation accuracy for the system with vector control and system with uncontrolled current.

5.1 Actual Torque and Maximum Torque

When the commutation of the motor is perfect, we will get maximum achievable torque, which is desired. The BLDC motor consists of three phases. Each phase contributes to the overall torque generation by the motor. The torque generation in each phase is a sinusoidal function. But the overall torque generated by the three phases together is a linear function. We can calculate the torque production of the motor from the current in the phases. However, current in each phase is also a sinusoidal function. To calculate the overall torque generated from phase current we can use equation (3.24). If we know the peak current in any phase, assuming the current flow in all phases are same, then using the per phase back-emf constant of the motor we can determine the torque generated from equation (3.24). If the peak current in the phases is I_P , the back-emf constant of the motor is k_b , and the torque generated is T , then from equation (3.24) we get

$$T = \frac{3}{2} k_b I_p. \quad (5.1)$$

This torque is the maximum achievable torque. Notice, this is a linear relationship. However, the actual torque in the motor is not linear with current. We used equation (3.21) in the simulation to generate the torque, which is also a nonlinear equation. The maximum torque equation is based on accurate commutation. So, if the commutation is not perfect, we will see the torque generated is not the same as maximum torque in the actual system or in our case in the simulation.

Now, if the maximum torque generated is T_{max} , we can rewrite the linear torque equation as,

$$T_{max} = \frac{3}{2} k_b I_p. \quad (5.2)$$

If the actual torque generated is T_{actual} then from the ratio of actual torque to maximum torque, we can determine whether or not the motor commutation is accurate or not. If the commutation is perfect then this ratio should be 1 or close to 1. Let us name this ratio as ‘torque ratio’. Thus, torque ratio can be defined as

$$torque_ratio = \frac{T_{actual}}{T_{max}}. \quad (5.3)$$

We can run the simulation for a specific speed command. And from the current scope of the simulation, we can find the peak current in motor phases. Then using the value for k_b , we can determine T_{max} . Also, from the torque scope of the simulation, we can find the actual torque generated by the motor. Thus, for the system with the uncontrolled current, we get the data listed in Table 5.1. For the system with vector control we get torque data listed in Table 5.2.

Table 5.1: Torque Data from Simulation of System with Uncontrolled Current.

Angular Speed, ω (rad/s)	Peak Current, I_p (Amps)	Maximum Torque, T_{max} (N-m)	Actual Torque, T_{actual} (N-m)	Torque Ratio (T_{actual}/T_{max})
100	0.38	2.92E-03	2.93E-03	1.00
250	0.96	7.41E-03	7.31E-03	0.99
500	1.98	1.53E-02	1.46E-02	0.96
750	3.13	2.41E-02	2.19E-02	0.91
1000	4.47	3.45E-02	2.92E-02	0.85
1250	6.10	4.71E-02	3.65E-02	0.77
1500	8.18	6.31E-02	4.37E-02	0.69
1750	10.93	8.43E-02	5.10E-02	0.60
2000	14.66	1.13E-01	5.84E-02	0.52

Table 5.2: Torque Data from Simulation of System with Vector Control.

Angular Speed, ω (rad/s)	Peak Current, I_p (Amps)	Maximum Torque, T_{max} (N-m)	Actual Torque, T_{actual} (N-m)	Torque Ratio (T_{actual} / T_{max})
100	0.3849	2.97E-03	2.97E-03	0.9986
250	0.9621	7.42E-03	7.41E-03	0.9988
500	1.924	1.48E-02	1.48E-02	0.9985
750	2.885	2.23E-02	2.22E-02	0.9988
1000	3.845	2.97E-02	2.96E-02	0.9989
1250	4.804	3.71E-02	3.70E-02	0.9989
1500	5.763	4.45E-02	4.44E-02	0.9985
1750	6.719	5.18E-02	5.18E-02	0.9984
2000	7.675	5.92E-02	5.91E-02	0.9982

Now, from Table 5.1, plotting speed and torque ratio we get Figure 5.1, torque ratio vs. angular speed for the system with uncontrolled current. From Table 5.2, plotting speed and

torque ratio we get Figure 5.2, torque ratio vs. angular speed for the system with vector control.

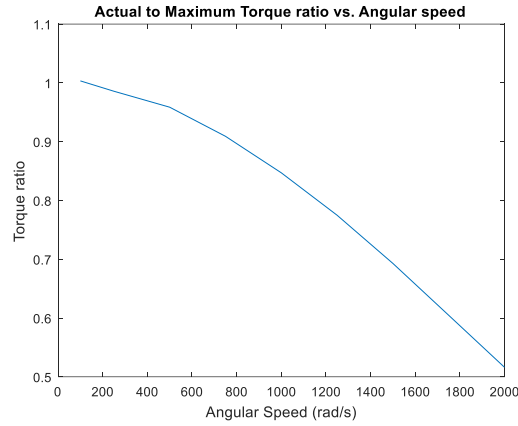


Figure 5.1: Torque Ratio Vs. Angular Speed for System with Uncontrolled Current.

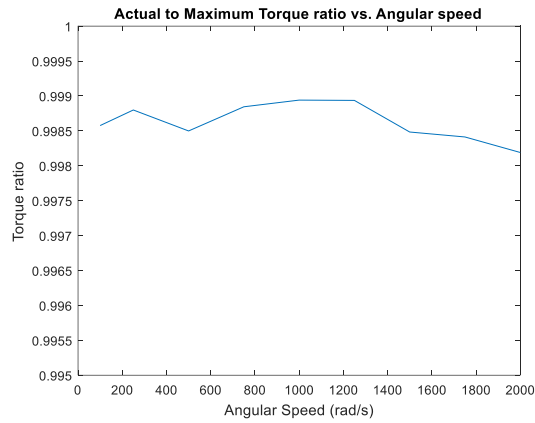


Figure 5.2: Torque Ratio Vs. Angular Speed for System with Vector Control.

From Figure 5.1 we can see that as the speed increases the torque ratio of the system with uncontrolled current decreases. At lower speeds, the value of the torque ratio is almost 1. Until 800 rad/s the torque ratio is more than 0.9. Or in other words, the torque generated by the motor is more than 90% of the maximum torque. But as the speed goes up the torque ratio reduces and at 2000 rad/s the torque generated is about 50% of the maximum torque.

This is due to the electrical dynamics of the motor. The electrical pole of the motor is R/L . For our motor, the value of this pole is 11,470 rad/s. As our motor has 14 magnetic poles, the speed of the electrical cycle will be 7 times of the mechanical angular speed. So, when the motor is running at an angular speed of 800 rad/s, the electrical speed is 5600 rad/s. Which is almost 50% of the electrical pole. So, when the electrical speed is more than 50% of the electrical pole the torque generation is less than 90% of the maximum torque. When the angular speed is 1640 rad/s the electrical speed is the same as the electrical pole. And at that speed we see the torque becomes 60% of the maximum torque. This is an indication of the commutation inaccuracy. So, from this observation, we can conclude that for the system with uncontrolled current the accuracy of the commutation reduces with increasing speed.

On the other hand, from Figure 5.2 we can see that the torque ratio for the system with vector control remains almost 1 for all the speeds in the same speed range. Although we see some ups and downs in the plot and the plot is moving downwards at the higher speeds, the changes are very small in value and therefore we can consider the torque ratio remains almost the same throughout the chosen speed range. So, we can conclude that for the system with vector control, the commutation is near perfect and therefore the motor is producing maximum possible torque.

In order to the commutation to be accurate the current in the motor phases must have a value that will produce the maximum torque. If the current peak is not occurring at the right place then we see the motor generating a torque lower than the maximum value. So, if the commutation of the motor is not right then the currents in the motor phases will be out of phase with the input voltage to the motor. From the simulation, we can calculate the phase

shift of the currents with the input voltage. For example, for phase A, plotting the input voltage and current in the same figure we get Figure 5.3.

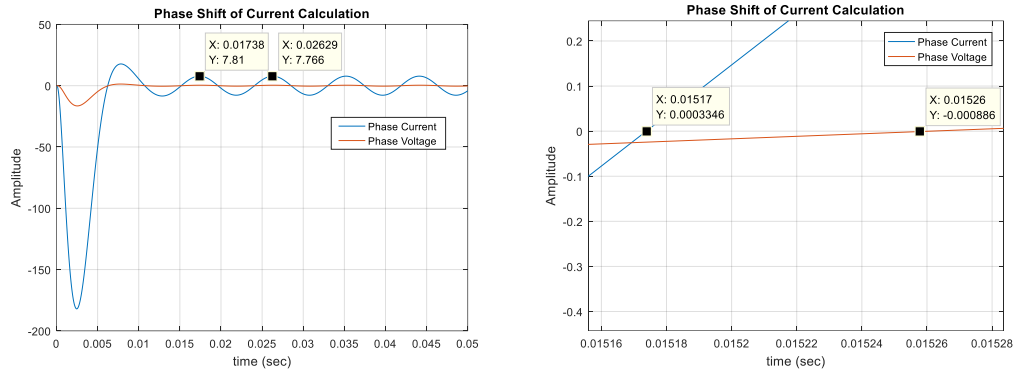


Figure 5.3: Calculating Phase Shifts of Motor Current.

From Figure 5.3 we get,

Time difference of two peaks = $(0.02629 - 0.01738) = 8.9 \text{ ms}$

Time difference of intersecting the zero line = $(0.01526 - 0.01517) = 0.09 \text{ ms}$

So, phase shift = $(0.09 * 360^\circ) / 8.9 = 3.64^\circ$

Here, the angular speed = 100 rad/s.

Similarly, running the simulation with increasing speeds and calculating the phase shifts of current we get Table 5.3 and Table 5.4 for the system with uncontrolled current and system with vector control respectively.

Table 5.3: Phase Shift of the Current for System with Uncontrolled Current.

Speed (rad/s)	100	250	500	750	1000	1250	1500	1750	2000
Phase Shift (deg)	3.64	9.11	18.18	24.57	32.36	37.66	41.90	46.68	52.66

Table 5.4: Phase Shift of the Current for System with Vector Control.

Speed (rad/s)	100	250	500	750	1000	1250	1500	1750	2000
Phase Shift (deg)	0.002	4.608	9.015	12.814	17.536	21.917	26.061	27.492	32.179

Now, from Table 5.3, plotting speed and phase shifts of the current we get Figure 5.4, current phase shift vs. angular speed for the system with uncontrolled current. And from Table 5.4, plotting speed and torque ratio we get Figure 5.5, current phase shift vs. angular speed for the system with vector control.

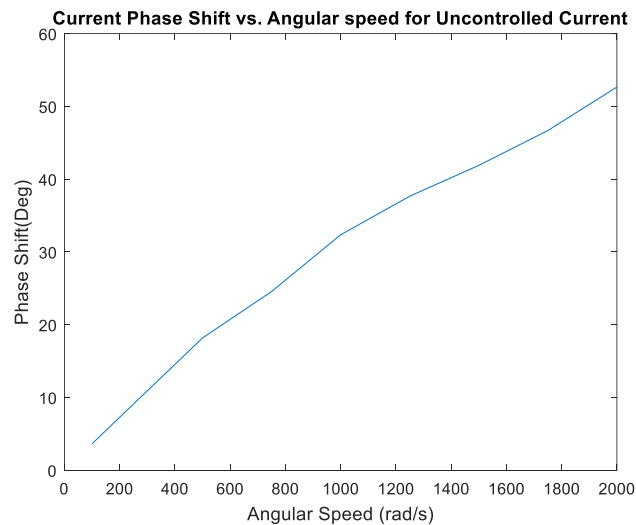


Figure 5.4: Simulated Phase Shift of Current for System with Uncontrolled Current.

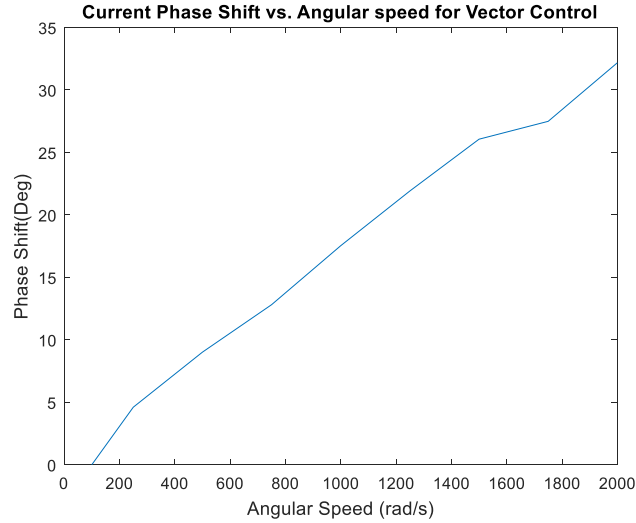


Figure 5.5: Simulated Phase Shift of Current for System with Vector Control.

From Figure 5.4 and Figure 5.5, we can see that with increasing speeds phase shift of the motor current increases for both of the systems. But this phase shift is much higher for the system with uncontrolled current. Which means the commutation accuracy is better in the system with vector control for the given speed range. These outcomes are the same as what we observed in Figure 5.1 and Figure 5.2.

So, in general, we can conclude that the commutation is better in the system with vector control. However, the commutation is not as bad in the system with uncontrolled current for a certain speed range. As mentioned before the torque generation of our motor is more than 90% of the maximum torque for the system with the uncontrolled current until 800 rad/s. This speed range can vary with a different motor. But there will always be a speed range for which the motor will produce more than 90% of the maximum torque or the phase shift in the current will not be big. So, if there is an application where it's not necessary to drive the system beyond this speed, then the uncontrolled current method can be used.

5.2 Computing Delay

Until now we didn't introduce any external delay to our simulation. We simulated our system in ideal condition, assuming we have a very fast computer that performs all the necessary calculations and controlling commands without adding any delay to the system. But in reality, the computer adds delays to the system. And if we use a microcontroller as our controller then it, in fact, can add a significant delay, as microcontrollers usually run with a slower frequency. And also, there might be some other insignificant dynamics that we didn't consider in our modeling but can slow down our system. It is, therefore, important for us to add delay to the simulation to represent a realistic system. Because any delay to the system can affect the commutation of the motor. We will combine all the delays in one single block and assume that this delay will simulate all the delay that can take place in the real system including the computer delay. Now, adding the delay in our previous speed simulation blocks we get we get Figure 5.6 and Figure 5.7.

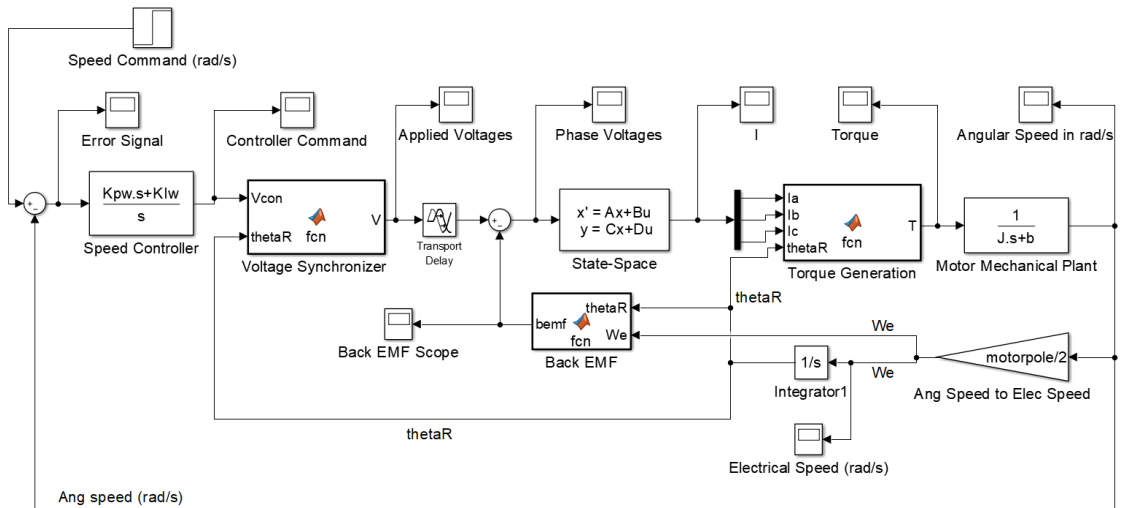


Figure 5.6: Simulation Model with Delay for System with Uncontrolled Current.

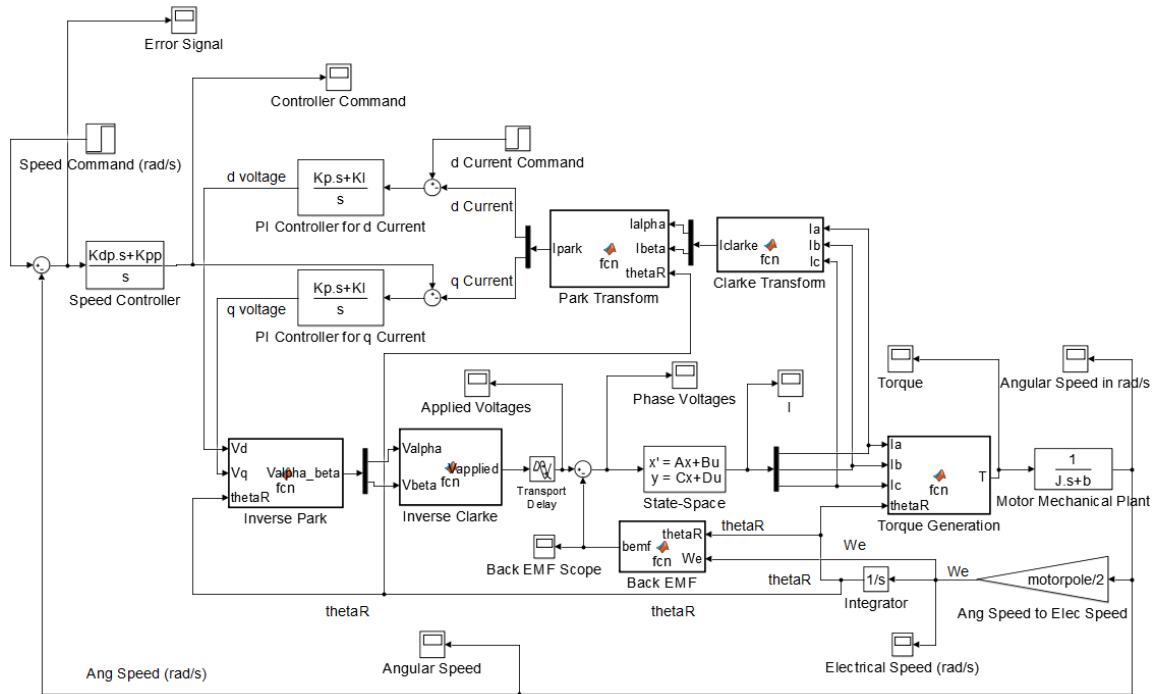


Figure 5.7: Simulation Model with Delay for System with Vector Control.

Running the simulations with a speed command of 100 rad/s and with zero transport delay we get the following responses as shown in Figure 5.8 and Figure 5.9.

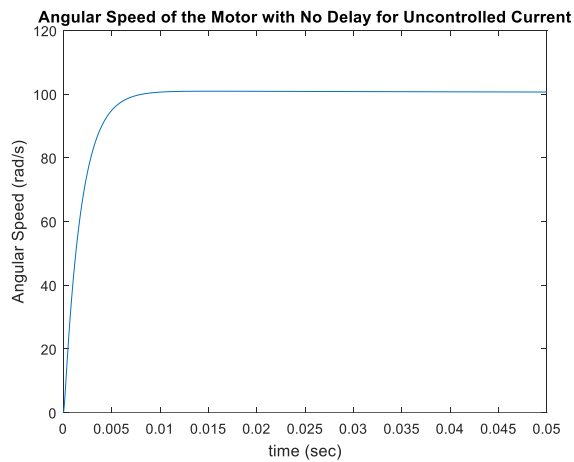


Figure 5.8: Simulated Angular Speed of the Motor with No Delay for Uncontrolled Current System.

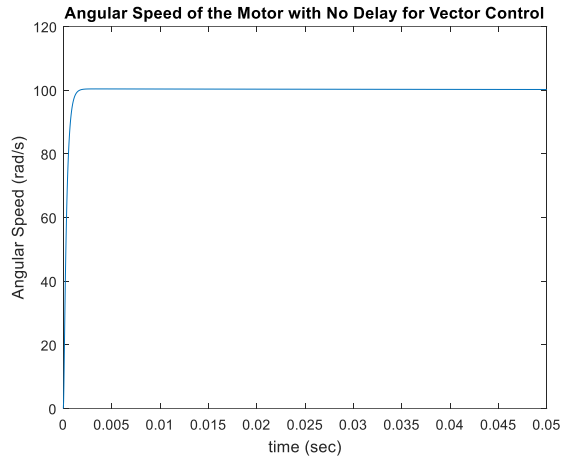


Figure 5.9: Simulated Angular Speed of the Motor with No Delay for Vector Control System.

Now, running the simulations with the same speed command with a transport delay of 0.001 sec we get the responses as shown in Figure 5.10 and Figure 5.11.

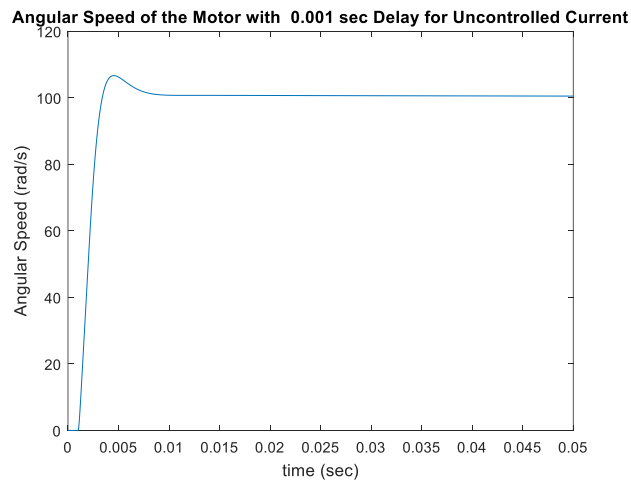


Figure 5.10: Simulated Angular Speed of the Motor with 0.001 Sec Delay for Uncontrolled Current System.

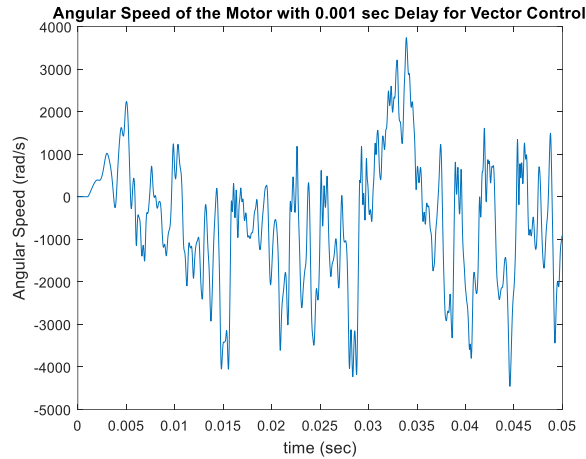


Figure 5.11: Simulated Angular Speed of the Motor with 0.001 Sec Delay for Vector Control System.

As can be seen from Figure 5.11 the system with vector control became unstable with a delay of 0.001 sec. On the other hand, the system with uncontrolled current is stable and the motor smoothly reaches the speed commanded with small overshoot, as shown in Figure 5.10. So, it is clear that the system with uncontrol current can handle external delays better than the system with vector control. This means uncontrolled current method will be more suitable for running with a slower computer, such as a microcontroller. This idea was also predicted by the frequency response analysis discussed in Chapter 4. Comparing Figure 4.5 and Figure 4.11 we could predict that the uncontrolled current system would handle external delays better as it has better phase margin. Also, comparing the delay margins from these two figures we can do the same prediction. And the delay margin in Figure 4.5 explains why the system with vector control becomes unstable with a delay of 0.001sec. The delay margin in Figure 4.5 is 0.000113 sec. Which means a delay of 0.001 sec is greater than the margin and therefore the system cannot handle it and becomes unstable.

Now, let's reduce the delay time to 0.0001 sec as the system with vector control cannot run with a delay of 0.001 sec. With 0.0001 sec delay and the same speed command used before we get the responses from two simulations shown in Figure 5.12 and Figure 5.13.

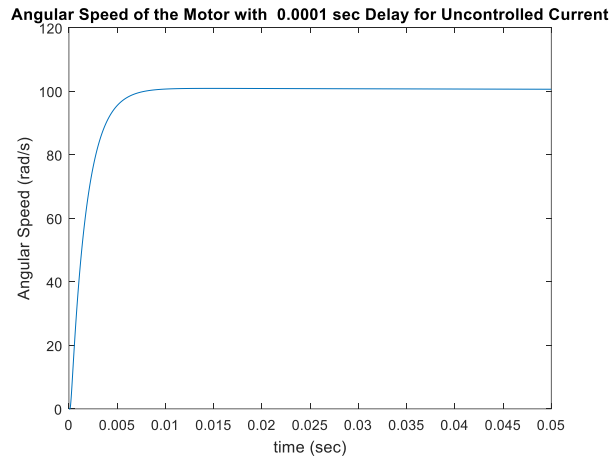


Figure 5.12: Simulated Angular Speed of the Motor with 0.0001 Sec Delay for Uncontrolled Current System.

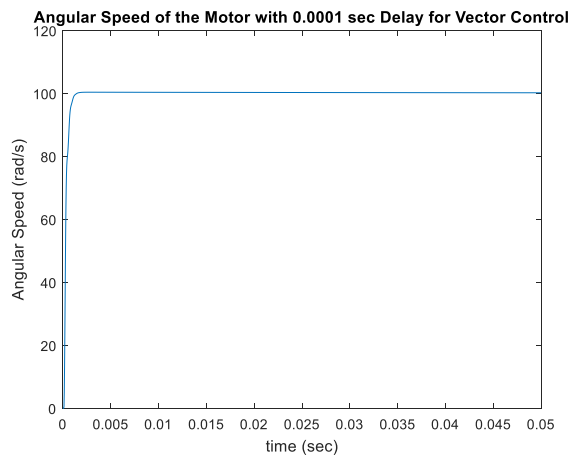


Figure 5.13: Simulated Angular Speed of the Motor with 0.0001 Sec Delay for Vector Control System.

As can be seen from Figure 5.12 and Figure 5.13 both of the systems are stable. Also, both the systems are reaching to the commanded speed smoothly as they did with zero delays.

So, we will use a delay of 0.0001 sec to compare the two systems.

Table 5.5: Torque Data for Uncontrolled Current with Delay in the Simulation.

Angular Speed	Peak Current	Maximum Torque	Actual Torque	Torque Ratio
100	0.38	2.92E-3	2.92E-3	1
250	1.058	8.16E-3	7.32E-3	0.89
500	3.52	0.027	1.46E-2	0.54
750	6.95	0.053	2.21E-2	0.42
1000	21.14	0.16	3.024E-2	0.19

Table 5.6: Torque Data for Vector Control with Delay in the Simulation.

Angular Speed	Peak Current	Maximum Torque	Actual Torque	Torque Ratio
100	3.852E-1	2.97E-3	2.966E-3	0.996
250	9.671E-1	7.46E-3	7.416	0.993
500	1.962	0.015	0.014	0.933
750	3.001	0.023	0.0215	0.934
1000	4.077	0.031	0.029	0.932

Now, recreating the tables for torque data for uncontrolled current and vector control with delay added to the system we get Table 5.5 and Table 5.6. From Table 5.5 and Table 5.6 we get Figure 5.14 and Figure 5.15 respectively.

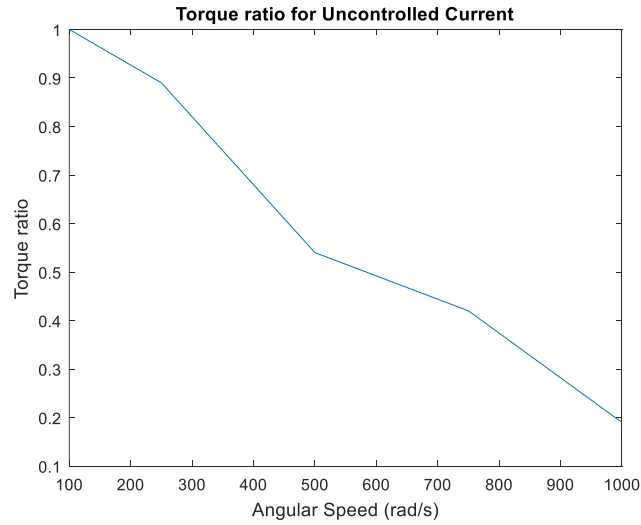


Figure 5.14: Torque Ratio for Uncontrolled Current with Delay in the Simulation.

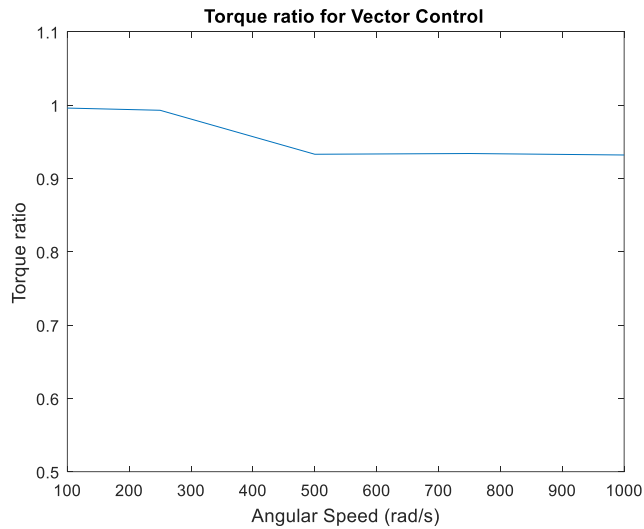


Figure 5.15: Torque Ratio for Vector Control with Delay in the Simulation.

From Figure 5.14 and Figure 5.15 we can see that the vector control still performs better. For both uncontrolled current and vector control the torque ratio is changed for the added delay to the system. Without delay the torque ratio was 0.6 for an angular speed of 200rad/s for uncontrolled current operation. But with the delay, the torque ratio now is less than 0.2 for an angular speed of 1000 rad/s for the same system.

Now, let us compare the phase shift of current with the input voltage in the two systems with the delay of 0.0001 sec. As we discussed earlier, from the current phase shift we can determine the accuracy of the commutation. Running the simulation with increasing speeds and calculating the phase shifts of current we get Table 5.7 and Table 5.8 for uncontrolled current and vector control, respectively.

Table 5.7: Phase Shift of Current with 0.0001 sec Delay for Uncontrolled Current.

Speed (rad/s)	100	250	500	750	1000
Phase Shift (deg)	11.124	25.794	49.551	66.667	78.348

Table 5.8: Phase Shift of Current with 0.0001 sec Delay for Vector Control.

Speed (rad/s)	100	250	500	750	1000
Phase Shift (deg)	7.420	17.573	35.274	52.764	65.513

Plotting the phase shift of current with angular speed from Table 5.7 and Table 5.8 we get Figure 5.16 and Figure 5.17, the simulated phase shift of current with 0.0001 sec delay for the system with uncontrolled current and vector control respectively.

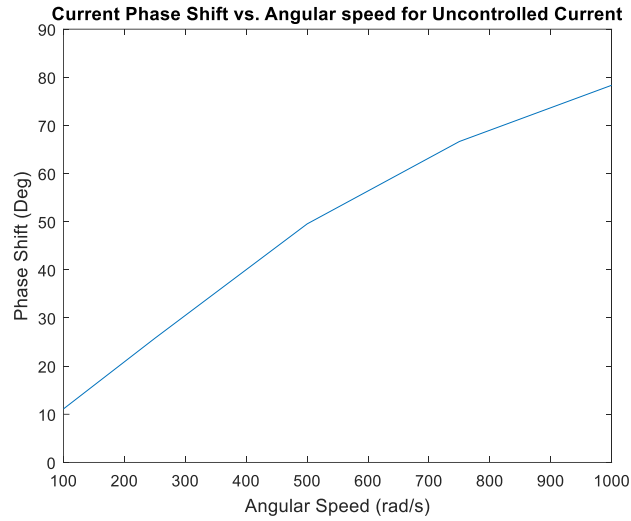


Figure 5.16: Simulated Phase Shift of Current with 0.0001 sec Delay for Uncontrolled Current.

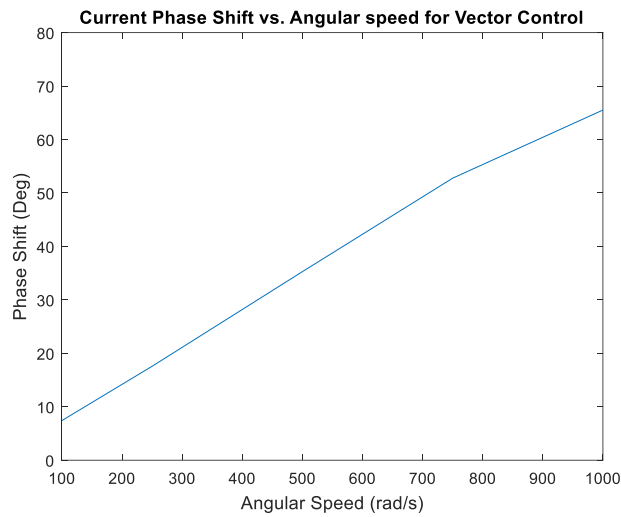


Figure 5.17: Simulated Phase Shift of Current with 0.0001 sec Delay for Vector Control.

From Figure 5.16 and Figure 5.17 we see that with a delay of 0.0001 sec, the current phase shift increases with increasing speeds for both vector control and uncontrolled current. The current phase shift is smaller in vector control for the same speed range, although smaller,

these values of phase shifts are closer to the uncontrolled current. Also if we compare Figure 5.16 and Figure 5.17 with Figure 5.4 and Figure 5.5 we can see that the phase shift in current increases with delay added for both systems. Which means vector control doesn't add many advantages in terms of commutation accuracy when there is a delay in the system. So, if we use a microcontroller with a low clock-speed, vector control and uncontrolled current have almost similar performance in terms of commutation.

Now, let us look at the phase shift of the back EMF with the input voltage for a delay of 0.0001 sec. If the back EMF is not in phase with the input voltage then the peak of the resultant voltage will not occur at the required rotor position to generate maximum torque. Therefore, it is important to study the phase shift of back EMF. With increasing speeds and calculating the phase shifts of current, we get Table 5.9 and Table 5.10 for uncontrolled current and vector control respectively.

Table 5.9: Phase Shift of Back EMF with 0.0001 sec Delay for Uncontrolled Current.

Speed (rad/s)	100	250	500	750	1000
Phase Shift (deg)	0.004	0.007	0.0035	0.0043	0.004

Table 5.10: Phase Shift of Back EMF with 0.0001 sec Delay for Vector Control.

Speed (rad/s)	50	100	250	500	750
Phase Shift (deg)	120.745	124.762	130.946	146.898	153.898

Plotting the phase shift of back EMF with angular speed from Table 5.9 and Table 5.10 we get Figure 5.18 and Figure 5.19, the simulated phase shift of back EMF with 0.0001 sec delay for the system with uncontrolled current and vector control respectively.

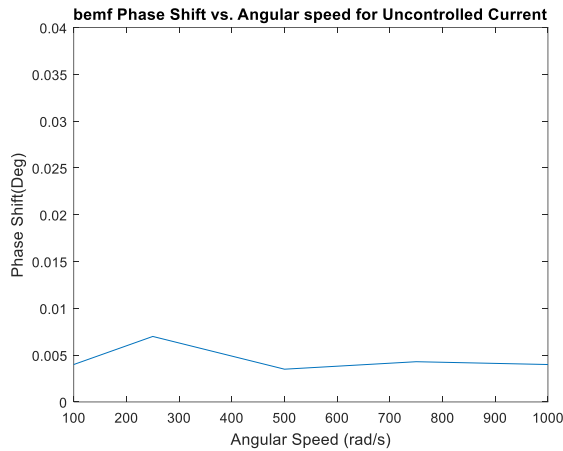


Figure 5.18: Simulated Phase Shift of Back EMF with 0.0001 sec Delay for Uncontrolled Current.

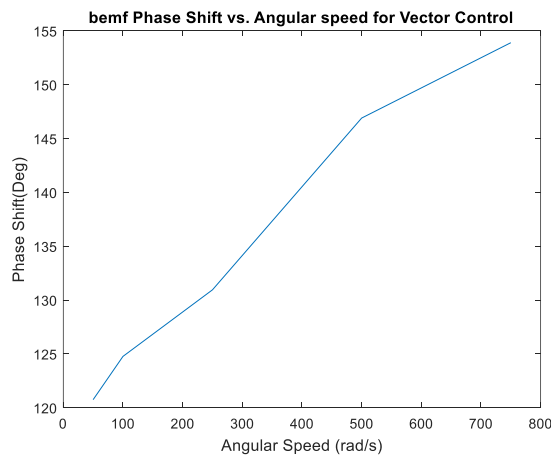


Figure 5.19: Simulated Phase Shift of Back EMF with 0.0001 sec Delay for Vector Control.

From Figure 5.18 we can see that phase shift of back EMF and the phase shift is almost zero for uncontrolled current and it doesn't increase with increasing speed for the given

speed range. And Figure 5.19 we see that the phase shift of back EMF is very prominent in vector control. Even in lower speeds, the back EMF has a very high phase shift for vector control. This can be explained by the phase margin from the frequency response analysis. The system with current control showed better phase margin than that of vector control. The delay is causing the back EMF to get out of phase. As the system with uncontrolled current has better delay margin, it can handle the delay and therefore the phase shift in back EMF for the uncontrolled current system is better than vector control.

Chapter 6 - Application of Uncontrolled Current Operation

In chapter 5 we have seen that the vector control is better than uncontrolled current operation in terms of commutation accuracy. However, we also discussed that the commutation accuracy of the uncontrolled current may be acceptable if it stays within a certain speed range. Also, the uncontrolled current system has better phase and delay margin which makes it suitable to be operated by a low-speed microcontroller. The vector control may not be able to work properly with a microcontroller system and may need a high-speed computer or controller. We have seen that the vector control system becomes unstable with a relatively large transport delay but the uncontrolled current system remains stable with the same delay. Which gives the uncontrolled current system advantage over the vector control system. And as it can be run by a microcontroller, it can be used in simpler applications where the efficiency and operating speed may not be a very big issue such as laboratory equipment for an introductory control theory course. In this chapter, we will only focus on the system with uncontrolled current and its application. We will perform various experiments and analysis on the system and establish the relationship between the model and the simulated actual system.

6.1 Saturation

Until now we used our simulation models to compare vector control with the uncontrolled current method. Now, we want to use the simulation model with uncontrolled current method to perform experiments. But, in order for us to represent the actual system, we need to make the simulation realistic. This is why we should include saturation in our simulation. Without saturation, the controller can command any amount of voltage to the motor to

achieve the required result. But a very high voltage command from the controller may not be realistic. Depending on the application the system will have a limitation on the voltage. So, it is wise to include a voltage saturation for the controller that will represent the actual system more realistically. This is especially important if this system is being used as introductory lab equipment. The voltage supply to the system, in this case, may not be very large. For our experiments in this chapter, we choose a voltage saturation upper limit of +12 volts and a lower limit of -12 volts. Figure 6.1 shows the simulation model for speed control model with uncontrolled current after the saturation block is included. From Figure 6.1 we can see the positioning of the saturation block.

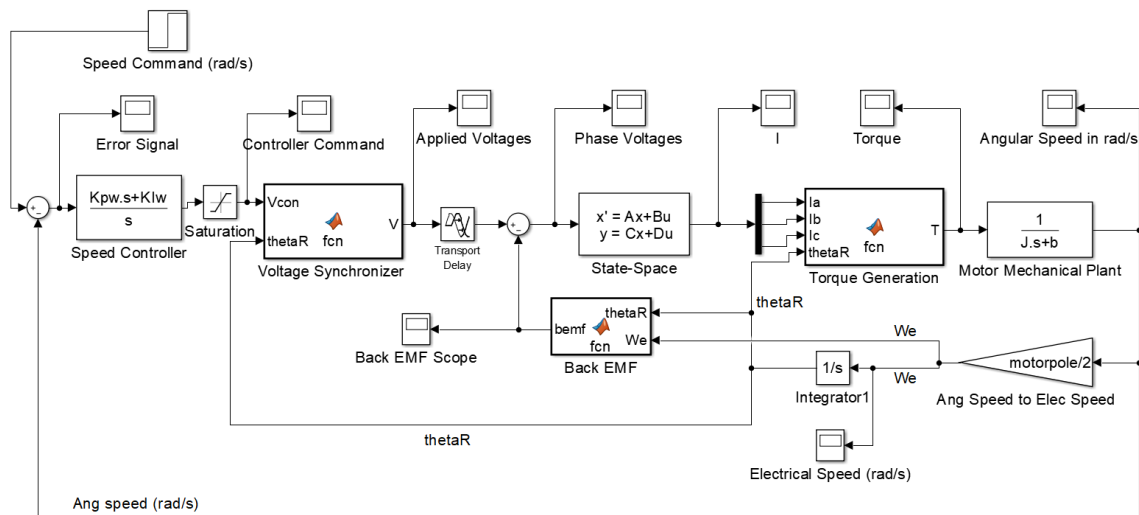


Figure 6.1: Simulation Block of Speed Control System with Voltage Saturation for Uncontrolled Current Operation.

And Figure 6.2 shows the simulation of position control model with the uncontrolled current after the saturation block is included.

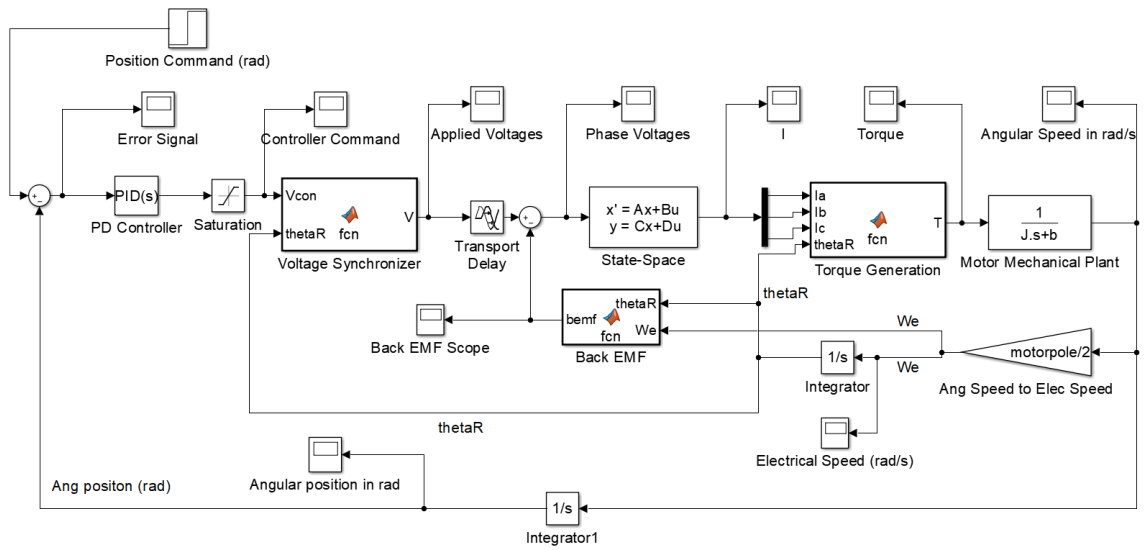


Figure 6.2: Simulation Block of Position Control System with Voltage Saturation for Uncontrolled Current Operation.

6.2 Speed Control Experiment with Uncontrolled Current

In this section, we will perform experiments on the speed control system. We will use the model derived in section 4.2 Speed Control Model with Uncontrolled Current to generate the theoretical response. And the output of the speed control simulation will be recorded as the response from the simulated actual system. We will use a combination of P and PI controllers with varying gains and speed commands to run these experiments. While choosing the gains and speed commands we need to make sure that the voltage command from the controller doesn't get saturated by the saturation block in the simulation. Otherwise, the response from our model and the actual system will not be the same.

6.2.1 Speed Control with Proportional Controller

The upper and lower limit of our voltage saturation is +12 volts and -12 volts respectively. So, we have to choose a combination of gain K_p and speed command so that the voltage command doesn't get saturated. Table 6.1 shows such a list of K_p gain and speed command combination. We will use these combinations to record responses from our model and the simulated actual system.

Table 6.1: Proportional Gain and Speed Command for Speed Control Experiment.

Speed (rad/s)	50	50	50	100	100	100	200	200
Kp (volts- sec)	0.05	0.1	0.2	0.005	0.01	0.1	0.01	0.05
Voltage (Volts)	2.5	5	10	0.5	1	10	2	10

Now, using these gains and speed commands we get following theoretical and actual responses from the model and simulation.

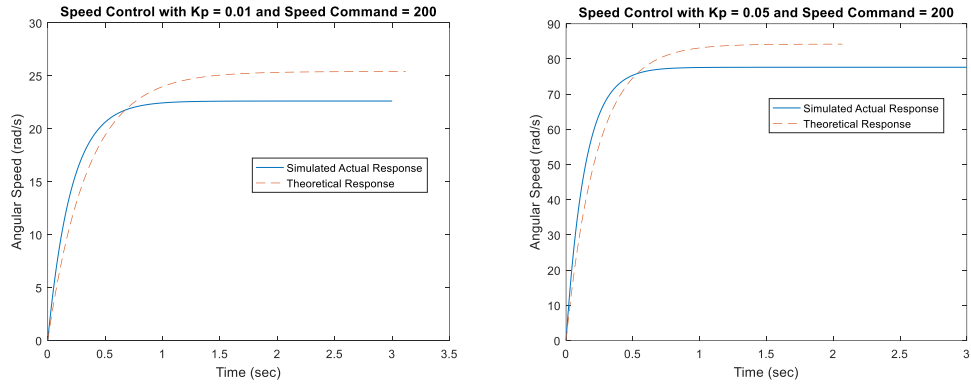


Figure 6.3: Speed Control Responses for Command = 200 and $K_p = 0.01, 0.05$.

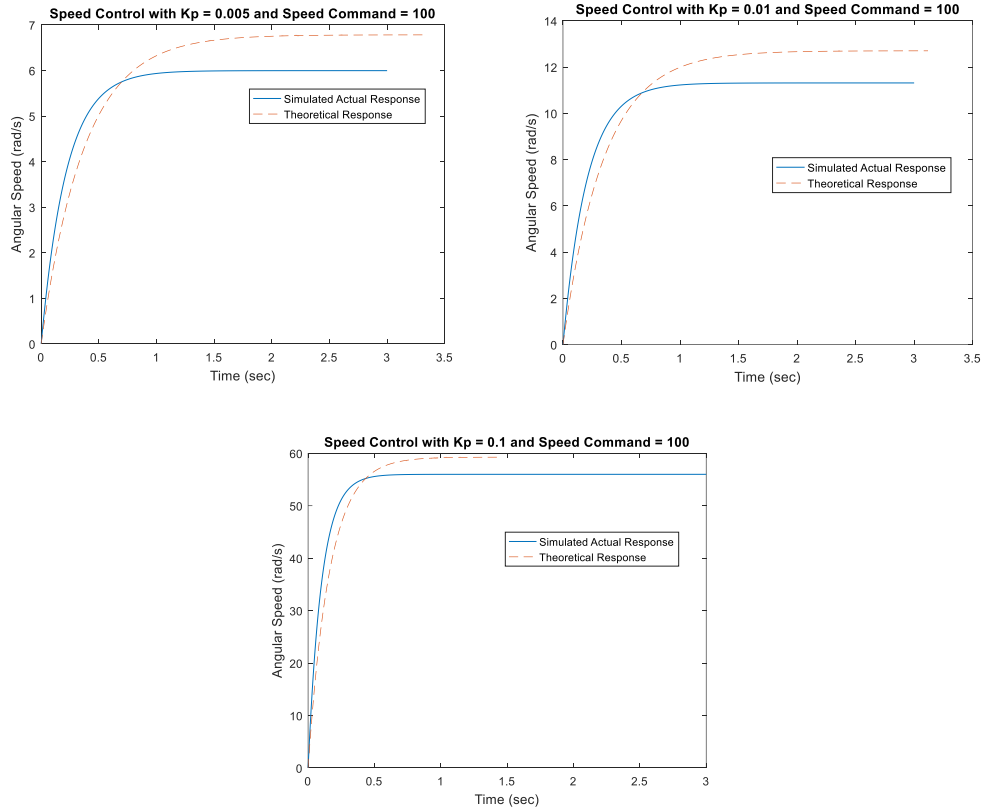


Figure 6.4: Speed Control Responses for Command = 100 and $K_p = 0.005, 0.01, 0.1$

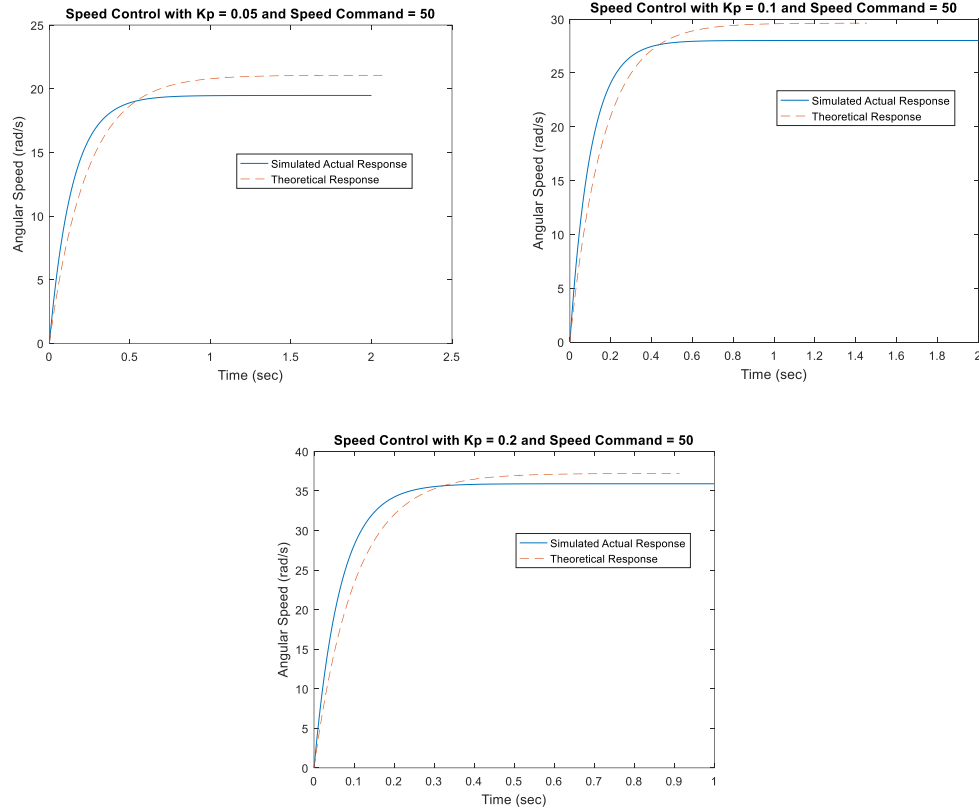


Figure 6.5: Speed Control Responses for Command = 50 and $K_p = 0.05, 0.1, 0.2$

In all of these responses, we see that the simulated system follows the model. We can see that there are some steady state errors in all of these responses. This is because we are using only a proportional controller. And as we know with only a proportional controller there will always be some steady state error. This is because, with just proportional gain, the system type of the speed control system is zero. And this is why for a step input we see an error in the steady state.

6.2.2 Speed Control with Proportional-Integral Controller

Now, let us use a PI controller for speed control. For this purpose, we are going to use the speed command controller gain combinations as shown in Table 6.2.

Table 6.2: P-I Gains and Speed Command for Speed Control Experiment

Speed (rad/s)	100	100	100	100	50	50
K_p (volts-sec)	0.001	0.001	0.05	0.05	0.01	0.1
K_I (volts-sec ²)	0.1	1	0.1	1	0.1	1

Using Table 6.2, from simulation and the model of the system we get the following speed control responses.

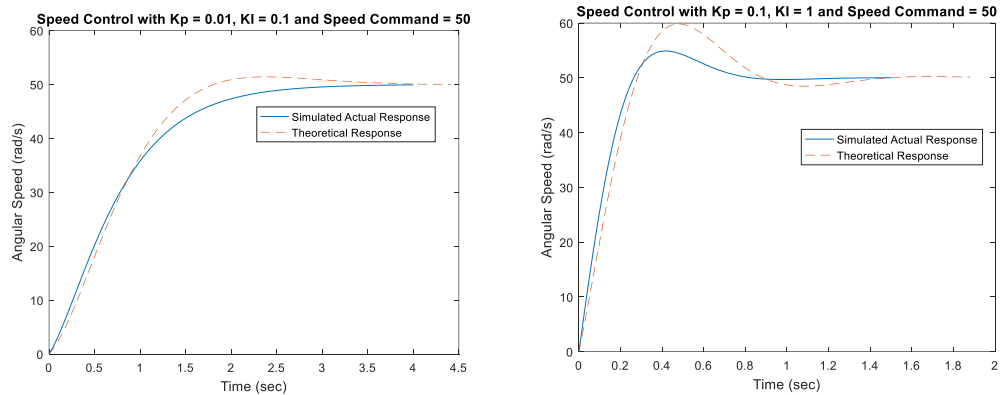


Figure 6.6: Speed Control Responses for Command = 50 with various PI Controllers.

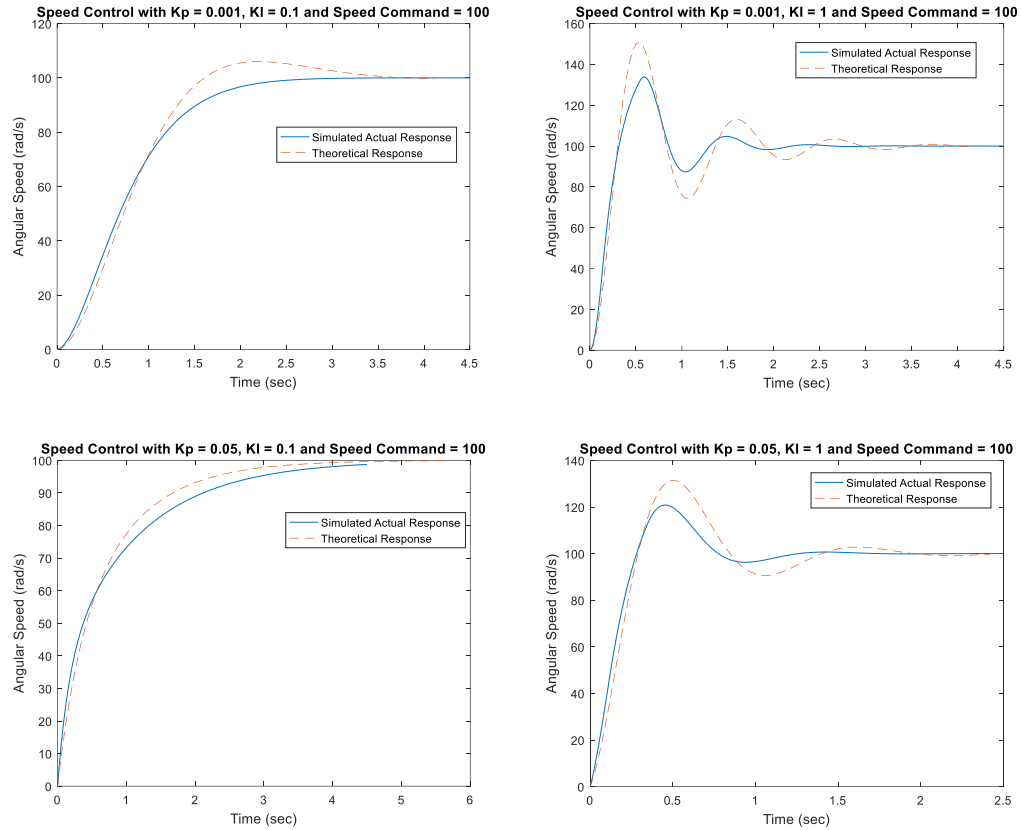


Figure 6.7: Speed Control Responses for Command = 100 with various PI Controllers.

As can be seen from Figure 6.6 and Figure 6.7 there is a good match between the theoretical and simulated actual responses. And unlike the responses with only proportional control here we don't see any steady state error. This is because with PI controller the speed control system has system type 1. This is why for step inputs we have zero steady state error.

6.3 Position Control Experiment with Uncontrolled Current

In order to perform experiments on the position control system, we will use the model developed in section 4.4 and the simulation shown in Figure 6.2.

6.3.1 Position Control with Proportional Controller

We select the position command and the proportional gain in such a way that it doesn't saturate the system. As we know our system has a saturation upper limit of +12 volts and a lower limit of -12 volts. The combination of proportional gain and position command is shown in Table 6.3.

Table 6.3: Position Control Experiment Command and Proportional Gain.

Command (rad)	10	50	100	300
K_p (volt/rad)	1	0.2	0.1	0.001

Now, using Table 6.3, from simulation and the model we get the following theoretical and experimental responses, as shown in Figure 6.8.

From Figure 6.8 we see that the actual simulated response follows the theoretical responses. For higher position commands, the system takes more time to settle. This is because for higher commands the gain is reduced so that the controller voltage command doesn't get saturated.

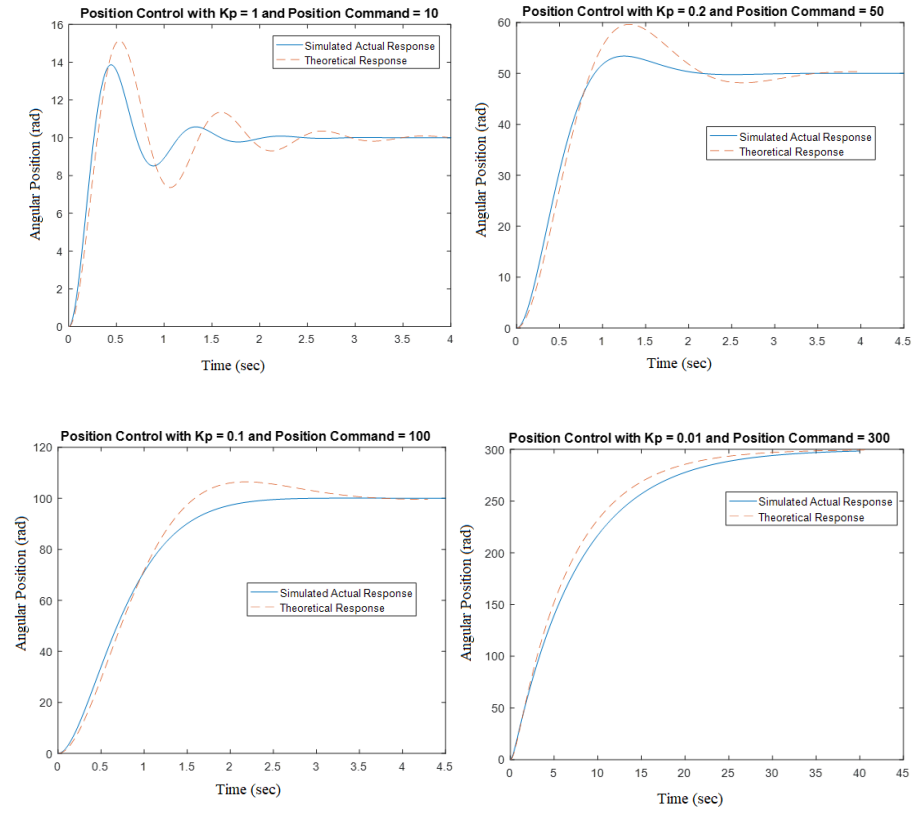


Figure 6.8: Position Control Responses for Various Commands and Proportional Gains.

6.3.2 Position Control with Proportional-Derivative Controller

Now, using a PD controller we will control the position and record the responses from the model and the simulation. We used the following gains and position commands as shown in Table 6.4.

Table 6.4: Position Control Experiment Command and P-D Gains.

Command (rad)	10	50	100
K_p (volt/rad)	0.5	0.2	0.05
K_d (Volt-sec/rad)	0.01	0.01	0.001

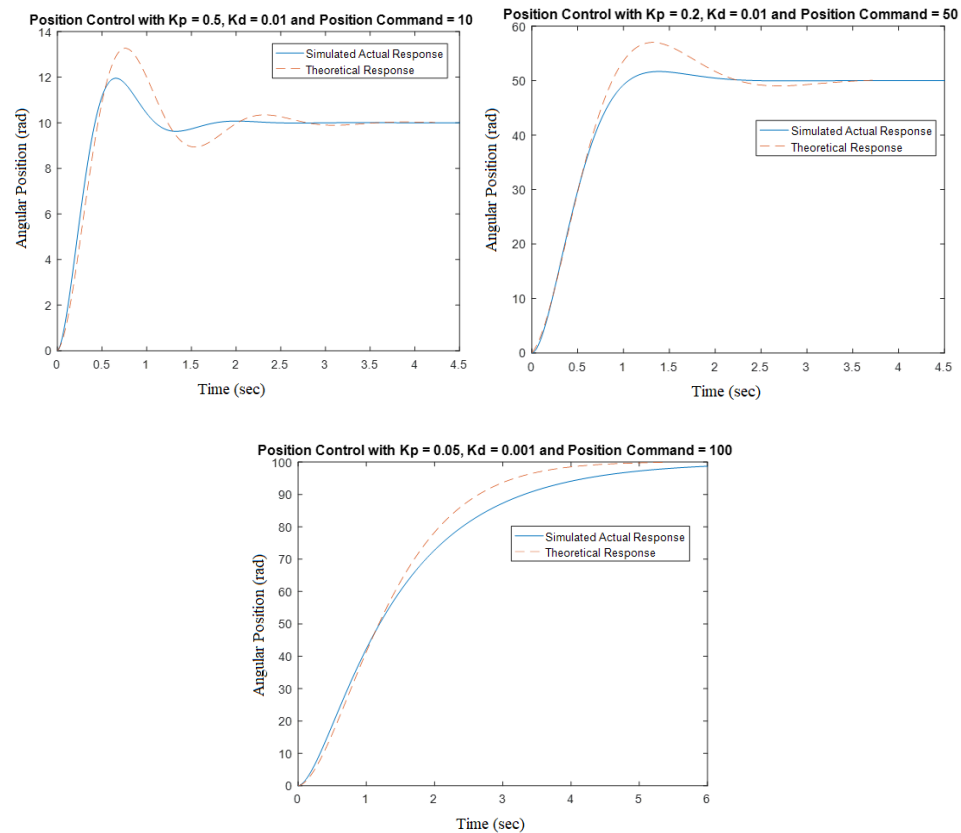


Figure 6.9: Position Control Responses for Various Commands and P-D Gains.

The position control theoretical and simulated actual responses found from the model and the simulation using the commands and gains in Table 6.4, is shown in Figure 6.9. And as can be seen, this experiment also shows satisfactory results, as the actual responses follow the theoretical response.

Chapter 7 - Conclusion

An overall comparison was carried out between the Uncontrolled Current Operation and the Field Oriented Control (FOC) or Vector Control Operation to drive a Brushless DC (BLDC) motor. In Chapter 4 the frequency response analysis was performed for the systems with both these methods. The frequency response analysis predicted that Vector Control method has a higher operating range compared to the Uncontrolled Current. So, vector control is more appropriate for high-speed operations. But the stability margin and delay margin for Vector Control is lower than that of Uncontrolled Current. Which indicates the delay handling capability of Vector Control is lower than that of Uncontrolled Current.

In chapter 5, the commutation accuracy of the BLDC motor was observed in the simulation for the system with Vector Control and Uncontrolled Current. It is seen that the Vector Control shows better commutation accuracy as it incorporates current control of the motor phases. This is why the system with Vector Control can produce maximum torque at a higher operating range. On the other hand, the maximum torque generation in the system with Uncontrolled Current reduces with increasing speed. However, the Uncontrolled Current system gives a very good torque output for a certain speed range. So, if the motor needs to run within this operating range, then the Uncontrolled Current method can be used.

In chapter 5 it is also seen that adding a delay to the system changes the system behavior significantly. The Vector Control system becomes unstable if the delay is larger. Whereas, the Uncontrolled Current system can operate with the same delay without any problem. The delay in the system also causes the back-EMF to fall out of phase with the input voltage

in the Vector Control System. On the other hand, the back-EMF in Uncontrolled Current remains in phase with the voltage. This is due to the higher delay margin of the Uncontrolled Current system, as predicted in the frequency response analysis. This indicates that a system with Uncontrolled Current Operation will be suitable to be controlled by a low-speed controller with large computing delay, such as a microcontroller. This can be helpful to achieve a low production cost of the system, as microcontrollers are typically cheaper. Also, for Uncontrolled Current, it's not required to measure the motor current, and therefore there is no need for a current sensor. This also reduces the production cost. On the other hand, vector control may be appropriate to work with a high-speed computer.

With low production costs, a system with Uncontrolled Current can be used as laboratory equipment in an introductory control theory course. In chapter 6 position and speed control experiments on system with the Uncontrolled Current is performed. The speed control experiment was performed with various P and PI controllers using varying speed commands. In the position control experiment, various P and PD controllers were used with varying position commands. Satisfactory results were observed for all of these experiments in model generated and simulation generate responses.

References

- [1] C. J. Bay and B. P. Rasmussen, "Exploring controls education: A re- configurable ball and plate platform kit," 2016 American Control Conference (ACC), Boston, MA, 2016, pp. 6652-6657. doi: 10.1109/ACC.2016.7526718

- [2] R. Krauss and J. Croxell, "A low-cost microcontroller-in-the-loop platform for controls education," 2012 American Control Conference (ACC), Montreal, QC, 2012, pp. 4478-4483. doi: 10.1109/ACC.2012.6314807

- [3] R. M. Reck, R. S. Sreenivas and M. C. Loui, "Assessing an affordable and portable laboratory kit in an undergraduate control systems course," Frontiers in Education Conference (FIE), 2015. 32614 2015. IEEE, El Paso, TX, 2015, pp. 1-4. doi:10.1109/FIE.2015.7344319

- [4] S. R. Smith, "Demonstrating introductory control systems concepts on inexpensive hardware," Master's thesis, Kansas State University, 2017.

- [5] M. Lazor and M. Štulrajter, "Modified field-oriented control for smooth torque operation of a BLDC motor," 2014 ELEKTRO, Rajecké Teplice, 2014, pp. 180-185. doi: 10.1109/ELEKTRO.2014.6847897.

- [6] J. R. Mevey, "Sensorless field-oriented control of brushless permanent magnet synchronous motors," Master's thesis, Kansas State University, 2009.

- [7] D. Schinstock, S. R. Smith, W. N. White, (2017), "Does Inexpensive Hardware Obfuscate Simple Experiments for Control Systems Laboratories?", American Control Conference, Seattle, WA.
- [8] D. J Black, "Development and feasibility of economical hardware and software in control theory application," Master's thesis, Kansas State University, 2017.
- [9] R. M. Reck and R. S. Sreenivas, "Developing a new affordable DC motor laboratory kit for an existing undergraduate controls course," 2015 American Control Conference (ACC), Chicago, IL, 2015, pp. 2801-2806. doi: 10.1109/ACC.2015.7171159
- [10] R. M. Reck, "Defining common aspects of undergraduate instructional laboratories for control systems," 2016 American Control Conference (ACC), Boston, MA, 2016, pp. 6646-6651. doi: 10.1109/ACC.2016.7526717

Appendix A - Code

Initialization.m

```
clc
motorpole = 14; %number of motor poles
Kp = 10; % proportional gain
KI = 100; % integral gain
J = 1.29e-5; % moment of inertia
b = 3e-5; % friction coefficient
R = 10.9; % resistance
Ll = 0.95e-3; % inductance
kt = 0.03; % torque constant
kb = 0.03; % back emf constant
Lmat = [2*Ll Ll; Ll 2*Ll];
A1 = [-2*R -R; -R -2*R];
B1 = [1 0 -1; 0 1 -1];
A = inv(Lmat)*A1; % state matrix
B = inv(Lmat)*B1; % input matrix
C = [1 0; 0 1; -1 -1]; % output matrix
D = [0 0 0; 0 0 0; 0 0 0]; % direct matrix
```

Torque Generation

```
function T = fcn(Ia,Ib,Ic,thetaR)
%#codegen
kt = 0.036/7;
T = -kt*Ia*sin(thetaR) - kt*Ib*sin(thetaR-120*pi/180) -
kt*Ic*sin(thetaR+120*pi/180);
```

Back EMF

```
function bemf = fcn(thetaR,We)
%#codegen
kb = 0.036/7;
bemf = [-We*kb*sin(thetaR); -We*kb*sin(thetaR-120*pi/180); -
We*kb*sin(thetaR+120*pi/180)];
```

Voltage Synchronizer

```
function V = fcn(Vcon,thetaR)
%#codegen
V = [-Vcon*sin(thetaR); -Vcon*sin(thetaR-120*pi/180); -
Vcon*sin(thetaR+120*pi/180)];
```

Clarke Transform

```
function Iclarke= fcn(Ia,Ib,Ic)
%#codegen
Iclarke = (2/3)*[3/2 0; sqrt(3)/2 sqrt(3)]*[Ia;Ib];
```

Park Transform

```
function Ipark = fcn(Ialpha,Ibeta, thetaR)
%#codegen
Ipark = [cos(thetaR) sin(thetaR); -sin(thetaR) cos(thetaR)]*[Ialpha;Ibeta];
```

Inverse Clarke Transform

```
function Vapplied= fcn(Valpha,Vbeta)
%#codegen
Vapplied = (3/2)*[2/3 0; -1/3 1/sqrt(3); -1/3 -1/sqrt(3)]*[Valpha;Vbeta];
```

Inverse Park Transform

```
function Valpha_beta = fcn(Vd,Vq, thetaR)
%#codegen
Valpha_beta = [Vd*cos(thetaR)-Vq*sin(thetaR); Vd*sin(thetaR)+Vq*cos(thetaR)];
```

Bode Plot Generator for Section 4.5

```
clc
J = 1.29e-5; % moment of inertia
b = 3e-5; % friction coefficient
R = 10.9; % resistance
L1 = 0.95e-3; % inductance
kt = 0.03; % torque constant
kb = 0.03; % back emf constant

%%
%%%%%%%%%%%%%%%%%%%%%%%%%%%%%%%%%%%%%%%%%%%%%%%%%%%%%%%%%%%%%%%%%%%%%%%% speed control with vector control %%%%%%%%% section 4.1
Gmec = tf(1,[J b]);
Gelec = tf(1,[L1 R]);
Kp = 10;
KI = 100;
Gci = tf([Kp KI],[1 0]); % current controller
KIw = 100;
Kpw = 10;
Gcw = tf([Kpw KIw],[1 0]); % speed controller
```

```

Gmotor = Gelec/(1+kb*kt*Gmec*Gelec);
Gvec = Gmotor*Gci/(1+Gmotor*Gci);
OL_vec_speed = Gcw*Gvec*kt*Gmec;
Gclw_vec = OL_vec_speed/(1+OL_vec_speed);
figure(1)
bode(OL_vec_speed)
title('Open Loop Speed Control System with Vector control');
figure(11)
bode(Gclw_vec);
title('Closed Loop Speed Control System with Vector control');

%%
%%%%%%%%%%%%%%%%%%%%%%%%%%%%%%%%%%%%%%%%%%%%%%%%%%%%%%%%%%%%%%%%%%%%%%%% section
4.2
OL_uc_speed = Gcw*Gmotor*kt*Gmec;
Gclw_uc = OL_uc_speed/(1+OL_uc_speed);
figure(2)
bode(OL_uc_speed)
title('Open Loop Speed Control System with Uncontrolled Current');
figure(12)
bode(Gclw_uc);
title('Closed Loop Speed Control System with Uncontrolled Current');

%%
%%%%%%%%%%%%%%%%%%%%%%%%%%%%%%%%%%%%%%%%%%%%%%%%%%%%%%%%%%%%%%%%%%%%%%%% section
4.3
free_int = tf(1,[1 0]);
Kpp = 10;
Kdp = 0.001;
Gcp = tf([Kdp Kpp],1); % position controller
OL_vec_pos = Gcp*Gvec*kt*Gmec*free_int;
Gclp_vec = OL_vec_pos/(1+OL_vec_pos);
figure(3)
bode(OL_vec_pos);
title('Open Loop Position Control System with Vector control');
figure(13)
bode(Gclp_vec);
title('Closed Loop Position Control System with Vector control');

%%
%%%%%%%%%%%%%%%%%%%%%%%%%%%%%%%%%%%%%%%%%%%%%%%%%%%%%%%%%%%%%%%%%%%%%%%% section
4.4
OL_uc_pos = Gcp*Gmotor*kt*Gmec*free_int;
Gclp_uc = OL_uc_pos/(1+OL_uc_pos);
figure(4)
bode(OL_uc_pos);
title('Open Loop Position Control System with Uncontrolled Current');
figure(14)
bode(Gclp_uc);
title('Closed Loop Position Control System with Uncontrolled Current');

```